ANNUAL REVIEWS

Annual Review of Materials Research

Mixed Ionic-Electronic Transport in Polymers

Bryan D. Paulsen,[1] Simone Fabiano,[2] and Jonathan Rivnay[1,3]

[1]Department of Biomedical Engineering, Northwestern University, Evanston, Illinois 60208, USA; email: jrivnay@northwestern.edu

[2]Laboratory of Organic Electronics, Department of Science and Technology, Linköping University, SE-601 74 Norrköping, Sweden

[3]Simpson Querrey Institute, Northwestern University, Chicago, Illinois 60611, USA

Annu. Rev. Mater. Res. 2021. 51:73–99

First published as a Review in Advance on May 4, 2021

The *Annual Review of Materials Research* is online at matsci.annualreviews.org

https://doi.org/10.1146/annurev-matsci-080619-101319

Keywords

polymer electrolytes, polyelectrolytes, conjugated polymers, conducting polymers, mixed conductor, mixed transport

Abstract

Polymeric mixed ionic-electronic conductors (MIECs) combine aspects of conjugated polymers, polymer electrolytes, and polyelectrolytes to simultaneously transport and couple ionic and electronic charges, opening exciting new applications in energy storage and conversion, bioelectronics, and display technologies. The many applications of polymeric MIECs lead to a wide range of transport conditions. Ionic and electronic transport are directly coupled through electrochemical doping, while the mechanisms of ionic and electronic transport depend on distinctly different chemical functionality, (macro)molecular structure, and morphology. Despite this, ionic and electronic transport are surprisingly tunable, independent of one another. We review the various types of polymeric MIECs, the mechanisms of ionic and electronic charge transport across conditions, and the interrelations between the two, with special emphasis on the unique aspects of polymeric MIEC transport phenomena.

1. INTRODUCTION

Initially, electronically conducting polymers and ionically conducting polymers were developed separately. Electronically conducting polypyrrole was discovered and reported in 1963 (1), though it was not until the independent discovery and report of electrically conducting polyacetylene in 1977 that electrically conducting conjugated polymers (CPs) received wider attention (2). Around roughly the same time, poly(ethylene oxide) (PEO) was found to be capable of dissolving salts (3) and displaying significant ion conduction (4). Both systems were very quickly recognized to have promise in electrochemical applications, and thus it was only a matter of time before polymeric materials were purposefully designed to leverage both electronic and ionic conduction simultaneously.

Polymer mixed ionic-electronic conductors (MIECs) were explicitly recognized and studied beginning in the late 1980s as potential battery electrodes (5). Since then, a robust field of organic MIECs has emerged (6), among which polymeric MIECs are the most successful. As soft solids, polymeric MIECs are mechanically, electrically, and chemically responsive in unique ways compared to traditional inorganic MIECs (6). Today polymer mixed conductors have been employed in light-emitting electrochemical cells (LEECs) (7), actuators (8), neuromorphic devices (9), bioelectronics (10), organic electrochemical transistors (11), iontronics (12), thermoelectrics (13), supercapacitors (14), battery electrodes (15), and electrochromics (16), to name a few. Polymeric MIECs are so broadly applicable due to ionic-electronic interactions that allow them to store and transduce (ionic and electronic) charge and signals, respectively.

It is instructive to look to the more established fields of ionic transport in polymer electrolytes/polyelectrolytes and electronic transport in doped organic semiconductors. However, the same ionic-electronic interactions that make polymeric MIECs attractive complicate mixed transport. The numerous insightful studies of mixed transport in polymers are spread across several decades and multiple disciplines; thus, we draw important connections across the literature to assemble a complete picture of the present body of knowledge of mixed transport in polymeric materials. Here, we describe the ion and electronic transport in polymeric MIECs from the dry to gelled state, with an emphasis on the deviations from the behavior of simple electronic or ionic conductors. Further, we highlight the unique synergetic effect on thermally driven charge transport.

2. IONIC TRANSPORT

The understanding of ionic transport in polymeric MIECs is dependent on the extensive work done studying electrically insulating polymer electrolytes and polyelectrolytes (**Figure 1*a*,*b***). In particular, the following section draws heavily on some classic texts (17, 18) and excellent recent reviews (19, 20). To survey ionic transport in polymeric MIECs, it is worthwhile to consider what chemical functionality allows for ions to dissolve in polymers, what phenomena drive ionic transport, the macromolecular motion that allows or facilitates said ionic transport, and various compositional environments in which ionic transport in polymeric MIECs occurs.

2.1. Ion Solvation

For a polymer to conduct ions, it must be able to dissolve a salt (i.e., a reduction of the Gibbs free energy of the salt dissolved in the polymer compared to the pure salt crystal). Poor solvation in polymeric MIECs manifests on the device level as ion injection and transport barriers and poor ionic-electronic coupling (e.g., charge storage or doping). In typical electrolytes, solvation of ions arises by hydrogen bonding in protic, high-dielectric-constant electrolytes (e.g., water) or by coordination to dipole containing functional groups in aprotic electrolytes (e.g., ether

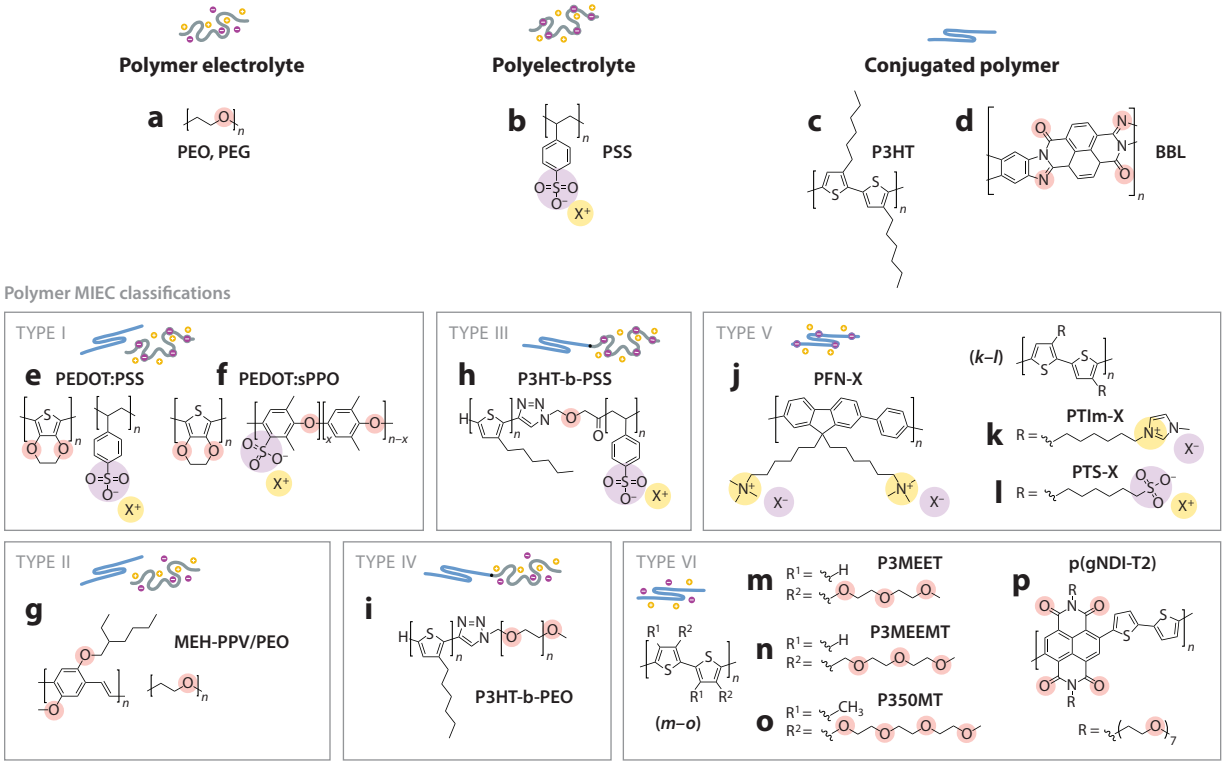

Figure 1

Chemical structures of representative (*a*) polymer electrolytes, (*b*) polyelectrolytes, (*c,d*) CPs, (*e,f*) type I CP/polyelectrolyte composites, (*g*) type II CP/polymer electrolyte blends, (*h*) type III CP-b-polyelectrolyte block copolymers, (*i*) type IV CP-b-polymer electrolyte block copolymers, (*j–l*) type V conjugated polyelectrolytes, and (*m–p*) type VI conjugated polymer electrolytes with anions, cations, and coordinating groups highlighted in purple, yellow, and pink, respectively. Abbreviations: BBL, backbone ladder; CP, conjugated polymer; MEH-PPV, poly[2-methoxy-5-(2-ethylhexyloxy)-1,4-phenylenevinylene]; MIEC, mixed ionic-electronic conductor; P3HT, poly(3-hexylthiophene); P3MEET, poly[3-(methoxyethoxyethoxy)thiophene]; P3MEEMT, poly[3-(methoxyethoxyethoxymethyl)thiophene]; P350MT, poly[3-oligo(oxyethylene)-4-methylthiophene]; PEDOT, poly(3,4-ethylenedioxythiophene); PEG, poly(ethylene glycol); PEO, poly(ethylene oxide); PFN-X, poly[9,9′-bis[6″-(N,N,N-trimethylammonium)hexyl]fluorene-alt-co-phenylene], where X is the anion; p(gNDI-T2), poly{[N,N′-bis(2-ethoxyethyl 2-(2-(2-methoxyethoxy)ethoxy)acetate)-naphthalene-1,4,5,8-bis(dicarboximide)-2,6-diyl]-alt-5,5′-(2,2′-bithiophene)}; PSS, poly(styrene sulfonate); PTIm-X, poly{3-[6-(1-methylimidazolium-3-yl)hexyl]thiophene-2,5-diyl}, where X is the anion; PTS-X, poly[6-(thiophen-3-yl)hexane-1-sulfonate], where X is the cation; sPPO, sulfonated poly(2,6-dimethyl 1,4-phenylene oxide).

oxygens in tetrahydrofuran) (**Figure 2*a,b***). The most common solid polymer electrolytes leverage periodically repeating ether oxygen groups to coordinate and solvate cations (**Figures 1*a*** and **2*c***), while anions are present but unsolvated. Alternatively, the polymer can be a component of the salt itself, paired with charge-balancing counterions (**Figures 1*b*** and **2*e***), as in the case of ionomers (<10% of the repeat units bear ionic charge) or polyelectrolytes (>10% of the repeat units bear ionic charge). Typical examples of polymer electrolytes and polyelectrolytes are PEO and poly(styrene sulfonate) (PSS), respectively (**Figure 1*a,b***).

Traditional CPs (**Figure 1*c,d***) tend to have low dielectric constants, lack (a high density of) ion-coordinating functional groups, and often contain long nonpolar alkyl side chains and thus do not readily dissolve most salts. Polymeric MIECs overcome this via the incorporation of ionic charge (polyelectrolytes) or coordinating groups (polymer electrolytes) (**Figure 2*d,f***). These groups can

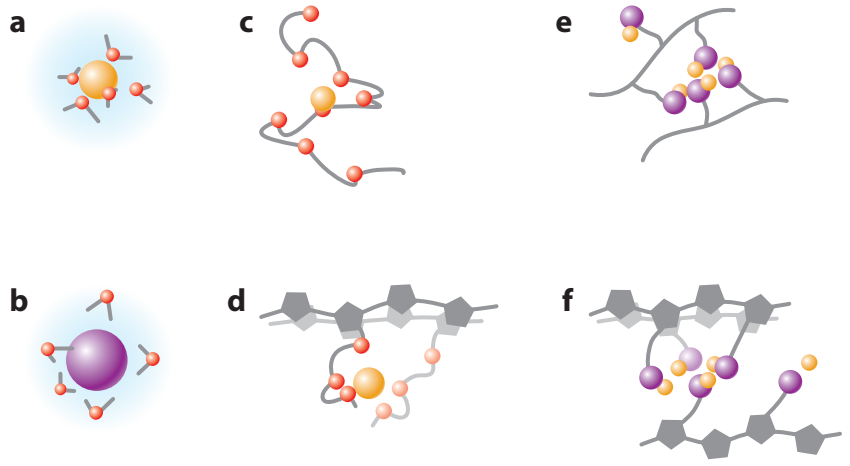

Figure 2

(*a*) Cation and (*b*) anion solvation by water in aqueous electrolytes, cation coordination by ether oxygens in (*c*) nonconjugated and (*d*) conjugated polymer electrolytes, and ion-pairing and aggregation in (*e*) nonconjugated and (*f*) conjugated polyelectrolytes. The cations, anions, and oxygens are displayed in yellow, purple, and red, respectively.

be present as side chains of the polymer backbone, covalently linked blocks, or distinct polymer electrolytes/polyelectrolytes that the CP has been composited with or templated on. This naturally gives rise to six types of polymer mixed conductor: (I) CP/polyelectrolyte blends, (II) CP/polymer electrolyte blends, (III) CP-b-polyelectrolyte block copolymers, (IV) CP-b-polymer electrolyte block copolymers, (V) conjugated polyelectrolytes, and (VI) CP electrolytes (**Figure 1**) (6).

For polyelectrolyte MIECs (types I, III, and V), the tethered ionic charge requires counterbalancing ions to maintain charge neutrality. Fixed ions are associated with oppositely charged counterions producing ion pairs, and ion pairs are energetically predisposed to cluster and aggregate (**Figure 1*e*,*f***) (21). In type VI conjugated polyelectrolytes, the ionic moieties are tethered via side chains (often alkyl in nature) to a rigid conjugated backbone (**Figures 1*d*** and **2*k–m***). The rigidity of the conjugated backbone and the energetic preference for π-π interchain interactions limit the degree of aggregation/clustering. Generally, ionic aggregates are confined to the lamellar spacing between π-stacked conjugated backbones (22–24).

Type II, IV, and VI polymer electrolyte MIECs most often employ (poly/oligo)ether chains, blocks, and side chains, respectively. Ion solvation requires a sufficient number of coordination sites, suitably spaced to allow chain conformation around the ion. In the linear polyethers, this ideal spacing is two carbons between each ether oxygen, as found in PEO (**Figure 1*a***). Alkali metal cations can reside in a PEO helix, coordinating with several ether oxygens (on average six in the case of Li^+) (**Figure 2*c***). Due to the low dielectric constant, these dissolved ions are poorly screened and can also associate into multiple ion aggregates directly as contact clusters or indirectly as solvent (chain) separated clusters. In PEO, anion coordination is negligible; as such, small halide ions are poorly soluble, while larger or polarizable anions (e.g., bis(trifluoromethane)sulfonimide) improve solubility (18).

In type I–IV polymeric MIECs (**Figure 1*e–i***), conjugated and ionic/ion-coordinating macromolecular components tend to phase segregate into CP-rich domains and polyelectrolyte/polymer electrolyte–rich domains, with ion dissolution occurring primarily in the latter. In type V and VI polymeric MIECs (**Figure 1*j–p***), ionic/ion-coordinating groups are evenly distributed along

the polymer and cannot naturally phase segregate. Due to phase segregation, type I–IV polymer MIECs tend to present compositional heterogeneity on the tens to hundreds of nanometers length scale, while length scale compositional heterogeneity in types V and VI is determined by the side chain length (2–4 nm). Often polymeric MIECs are semicrystalline, and the relative distribution of ions between the amorphous and crystalline domains is not known (25, 26).

In polymer mixed conductors, ions can also interact with electronic charge. Overall, electronic charge (holes or electrons) requires a counterbalancing dopant (anion or cation) to maintain charge balance. In polyelectrolyte MIECs (types I, III, and V), these can be some fraction of the fixed ionic charge on the polyelectrolyte. In type II, IV, and VI polymer mixed conductors, dopant ions are separately dissolved ionic species. Localized (trapped) electronic charge presents as a discrete site for ionic-electronic coordination (27). Conversely, delocalized electronic charge leads to a large increase in the dielectric constant (28) that works to screen particular ionic-ionic and ionic-electronic associations. In phase-separated polymer mixed conductors (types I–IV), the coordination between ionic and electronic charges can accumulate at the interface between the polyelectrolyte/polymer electrolyte–rich domains and the CP-rich domains (29, 30).

2.2. Ion Drift and Diffusion

Ionic transport occurs in response to electric field (drift/migration) and concentration gradient (diffusion) and, discounting convection, can be considered a summation of Ohm's law and Fick's law. For dilute systems in one dimension, the current density (J_{ionic}) due to ionic transport can be described as

$$J_{\text{ionic}} = \Sigma \left[e\,|z_i|\, n_i \mu_i \frac{\mathrm{d}\Phi}{\mathrm{d}x} + e z_i D_i \frac{\mathrm{d}n_i}{\mathrm{d}x} \right],$$

where e is the elementary charge, ϕ is the potential, z_i is the charge, n_i is the number density, μ_i is the mobility, and D_i is the diffusion coefficient of each ionic species. It follows that $\sigma_{\text{ionic}} = \Sigma[e|z_i|n_i\mu_i]$ is the ionic conductivity. In dilute conditions, n_i is easily convertible to the anion or cation concentration (c_i), and D_i and μ_i are interconvertible with the Nernst-Einstein equation,

$$D_i = RT\mu_i,$$

where R is the gas constant. However, assumptions of infinite dilution do not hold in polymer MIECs. Ion-ion interactions can produce neutral ion pairs (that can diffuse but do not migrate), net charged ion triplets, and larger clusters or aggregates that can be neutral or charged. Thus, raw anion and cation concentrations are not informative, and when known concentrations of each ion and multi-ion species are absent, anion and cation thermodynamic activities should be used. Additionally, depending on local pH, there may be non-negligible proton, hydronium, or hydroxide transport in hydrated or aqueous systems.

Given this complexity, ionic transport in polymer MIECs is often quantified as simple σ_{ionic} or molar fluxes. When diffusion coefficients or mobilities are reported, they should be considered apparent or effective unless rigorously proven otherwise. In certain systems, it can be helpful to consider ionic transport using Maxwell-Stefan diffusion (20) or in terms of an effective salt diffusion coefficient and transference number (19).

While in typical electrolytes electroneutrality requires the local cation and anion concentrations to be equal, this is not the case in polymeric MIECs, as holes or electrons can accumulate to counterbalance excess anions or cations:

$$F \sum z_i c_i + e n_{\text{holes}} - e n_{\text{electrons}} = 0,$$

where F is Faraday's constant, c_i is the individual ion concentrations, and n is the number density of electrons or holes. Thus, ionic transport in polymer MIECs can give rise to independent anion and cation concentration gradients (31), which are leveraged in LEECs (32).

2.3. Chain Motion

Solvated ion motion is necessarily coupled to the motion of the surrounding media. In liquid electrolytes, the bulk solvent molecules are highly mobile and reorganize around the ion and its solvation shell as they move together (i.e., vehicle transport), which manifests as a drag on ion motion that is proportional to the electrolyte viscosity. In polymers, ionic transport is similarly connected to motion of the surrounding macromolecules.

Except for low-molecular-weight oligomers, the solvating shell of coordination groups or ionic moieties covalently bound to the polymer cannot transport with the ion (i.e., no vehicle transport). Thus, the solvation shell is continually reforming as ions move between coordination sites through local motion of the polymer chains. On short time and length scales, polymer segmental motion can be described as an unentangled chain using the Rouse or Zimm model, while on longer time and length scales, the motion of an entire entangled polymer chain can be described using the reptation model (33). Uncoordinated ions (e.g., anions in PEO) still depend on chain motion to move through the available free volume of the polymer. Due to this dependence on chain motion, crystallinity is often detrimental to ionic transport.

When considering chain-coupled ion motion, it is instructive to consider the polymer persistence length (ℓp), which describes the length below which the polymer acts like a rigid rod. For example, ℓp for PEO is only 4 Å (**Figure 1*a***) (33, 34); thus, a single chain can conform around a cation and provide multiple sites for cation-ether oxygen coordination. Polystyrene has a $\ell p \approx$ 7.3 Å (33), while PSS (**Figure 1*b***) has a $\ell p \approx 12$ Å (35), as the aggregation of ion pairs results in longer rigid segments of polymer. The PEO ℓp is sufficiently short (i.e., the polymer is sufficiently flexible) such that segmental motion occurs close to the scale of individual ion-coordinating ether oxygens, allowing the cation to move while maintaining a highly coordinated solvation shell. PSS chains are not so flexible as to allow the individual motion of coordinating sulfonate ions, but they are flexible enough to bring neighboring ion aggregates in and out of close proximity with each other, allowing ion hopping.

Polymeric MIECs contain a high degree of conjugation, imparting increased chain rigidity. For example, regioregular poly(3-hexylthiophene) (P3HT) (**Figure 1*c***) in dilute solution displays a ℓp of 29 Å, over seven times that of PEO (36). In the solid state, this increases to a ℓp of 49 Å and 75 Å for amorphous and crystalline chains, respectively (37). Thus, conjugated chains are not able to conform themselves to particular ions due to the limited local segmental motion to assist ion motion. Fluctuations in the dihedral angle between repeat units [e.g., the ethylenedioxy rings on poly(3,4-ethylenedioxythiophene) (PEDOT)] may impart some small ability for coordinating sites to reorient in response to adjacent cations, particularly in amorphous domains (38, 39). As with ion solvation, in phase-separated systems (types I–IV), segmental motion in the nonconjugated polyelectrolyte/polymer electrolyte–rich domains promotes ionic transport. For nominally homogenous type V and VI polymer MIECs, the local motion of the ionic or ion-coordinating side chains enables ion motion.

Because of the dependence of ionic transport on polymer motion, the temperature dependence of σ_{ionic} often follows the same functional dependence as the Vogel-Fulcher-Tammann (VFT) formulation of viscosity near a materials glass transition temperature, T_g (40),

$$\sigma_{\text{ionic}} = \sigma_0 e^{\left(\frac{-B}{R(T-T_0)}\right)}.$$

While this is an empirical model, T_0 is generally related to T_g by a constant offset. Below (18) and far above (19) T_g, a simple Arrhenius relationship captures the temperature dependence of ionic conductivity (41):

$$\sigma_{\text{ionic}} = \sigma_0 e^{\left(\frac{-E_a}{RT}\right)},$$

where E_a is the activation energy of the ionic transport. In traditional CPs, the VFT relationship must be modified to account for the applied potential and the solubility mismatch of ions with CPs (42).

Despite the importance of thermal transitions in rationalizing ionic transport, the thermal properties of polymeric MIECs are not fully understood. In conjugated polyelectrolytes (type V), melt and glass transitions are counterion dependent (24). In type VI systems, thermal transitions are often not observed, despite clear crystallinity as assessed by X-ray scattering. In random copolymers of oligoethylene glycol and alkyl side chain monomers, an oligoethylene glycol fraction of 5% is sufficient to suppress all measurable thermal transitions, despite significant crystallinity being retained (43). In similar homopolymers, glass and multiple melt transitions are apparent when a methyl group separates the polythiophene backbone and the first side chain ether oxygen. Absent the methyl spacer, two glass transitions but no melting transitions were observed, despite the polymers showing crystallinity via diffraction (44). It is possible that the enthalpy of melting (ΔH_m) is suppressed in these systems or that the T_m is shifted beyond the degradation temperature.

2.4. Ionic Transport Environments

There are four general ionic transport conditions to consider: dry, hydrated, swollen by a contacting liquid electrolyte, and (hydro)gelled (**Figure 3**). These conditions arise from varied applications of polymeric MIECs, and each case presents unique characteristics that influence ionic transport.

2.4.1. Dry ionic transport. The dry condition consists simply of the mixed conducting polymer and dissolved ions, lacking liquid solvent molecules from ambient vapor or a contacting

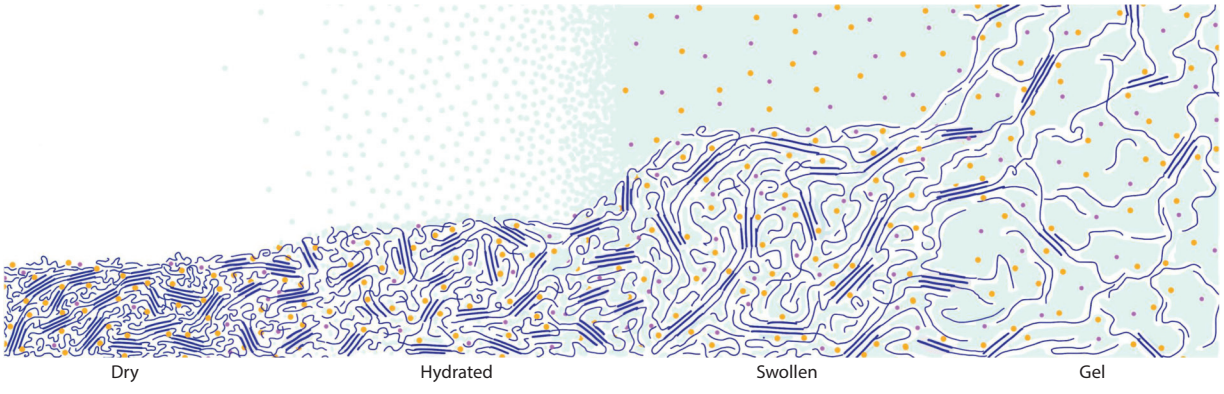

Figure 3

Illustration of the dry to hydrated to electrolyte swollen to gelled continuum of polymeric mixed ionic-electronic conductors. In the dry state, ion transport is wholly dependent on chain motion. Ambient solvent vapor or moisture can solvate ions and lead to significant swelling, which enhances ion transport. Contact with liquid electrolytes increases these effects. In the extreme case, such as a hydrogel, ion transport is essentially equivalent to that in a liquid electrolyte.

liquid electrode. These can be closed systems with a fixed total composition (e.g., LEECs) or open systems in contact with any ion sink/source (e.g., a solid polymer electrolyte) with a dynamic total composition (e.g., solid-state battery electrodes). In both cases, ionic transport is dependent on chain fluctuations, and extended conjugation is detrimental to ionic transport. Microphase-separated materials with flexible nonconjugated chains or blocks show the highest dry σ_{ionic} (40, 45–47). In type IV P3HT-b-PEO (**Figure 1*i***), σ_{ionic} of $\sim 5 \times 10^{-4}$ S/cm at 90°C is on par with pure PEO when normalized by ether oxygen content (40, 46, 47), indicating good connectivity between ion-coordinating sites (48). The type VI conjugated homopolymer electrolyte poly[3-oligo(oxyethylene)-4-methylthiophene] (P350MT) (**Figure 1*o***) with oligoethylene glycol side chains displays a decreased σ_{ionic} of 4×10^{-5} S/cm at similar temperatures due to decreased segmental motion from extended backbone rigidity (49), which likely manifests as a loss of coordination site connectivity (48).

Ion coordination pins chains, decreasing their fluctuations and increasing T_g with increasing ion concentration. For example, the T_g of P350MT (type VI) (**Figure 1*o***) increases ~90°C from neat to a salt loading of 0.35 cations per side chain ether oxygen (49). In addition, ion-ion interactions lead to a negative dependence of ion mobility on ion concentration. These compounding effects cause σ_{ionic} to rise with initial addition of salt, peak below 0.1 cation per ether oxygen, and decrease with additional salt in type II and VI polymeric MIECs (**Figure 4*a***) (44, 45, 49) similar to PEO (19).

In the dry state, type VI conjugated polyelectrolyte MIECs (**Figure 1*j–l***) display very low σ_{ionic} ($\sim 10^{-11}$ S/cm) (41, 50–52), as strong ion-ion interactions leave only ~0.1% of ions mobile (51), and the limited segmental motion due to conjugated backbone rigidity requires long hops between aggregates with large activation energies (0.8–1.6 eV) (41, 50, 51). Tripling the ion-containing side chain density on polyfluorene-based conjugated polyelectrolytes (**Figure 1*j***) halves the activation energy and increases σ_{ionic} by an order of magnitude ($\sim 10^{-10}$ S/cm) (51), presumably due to both an increase in mobile ions and a decrease in hopping distance between ion aggregates.

In electrically insulating polymer electrolytes, nonvolatile additives (crown ethers, tetraglyme, ionic liquids, etc.) have been shown to improve ionic transport by plasticizing the polymers (53), and creating a mobile solvation shell, à la vehicle transport. Initial studies of polymeric MIECs with ionic liquids (54, 55), sorbitol (56, 57), and crown ethers (58) have been promising.

2.4.2. Hydrated ionic transport. Hydration has a tremendous effect on ionic transport in polymer mixed conductors. Many polymer MIECs (especially types I, III, and V) show such low σ_{ionic} in the dry state that they can be considered as simply electrical (semi)conductors due to strong ion association with the polymer and limited chain motion. With hydration, water plasticizes chains, increasing chain motion, and begins to solvate the ions, partially displacing the polymer in the cation solvation shell (27). In conjugated polyelectrolytes, water dissociates the counterion. A sufficient degree of hydration produces a mobile solvation shell of water, allowing vehicle transport. At room temperature, the σ_{ionic} of conjugated polyelectrolytes (type VI) spans seven to eight orders of magnitude depending on the degree of hydration (**Figure 4*b***) (41, 52). PEDOT:PSS (type I) also shows similarly large increases in σ_{ionic} with increased hydration, and the degree of hydration in both can be quite large, 70–90 wt% at 90% relative humidity (RH) (52). At high levels of hydration, temperature-dependent σ_{ionic} deviates from VFT or Arrhenius behavior (41).

The σ_{ionic} of type I materials with high water content is quite high (10^{-3}–10^{-2} S/cm) (**Figure 5**) (41, 52, 59–61). These conductivities approach those of the equivalent aqueous electrolytes. As many polymeric MIECs incorporate poly(4-styrenesulfonic acid) (PSSH), parallel proton transport via the Grotthuss mechanism likely becomes significant in the highly hydrated state (62).

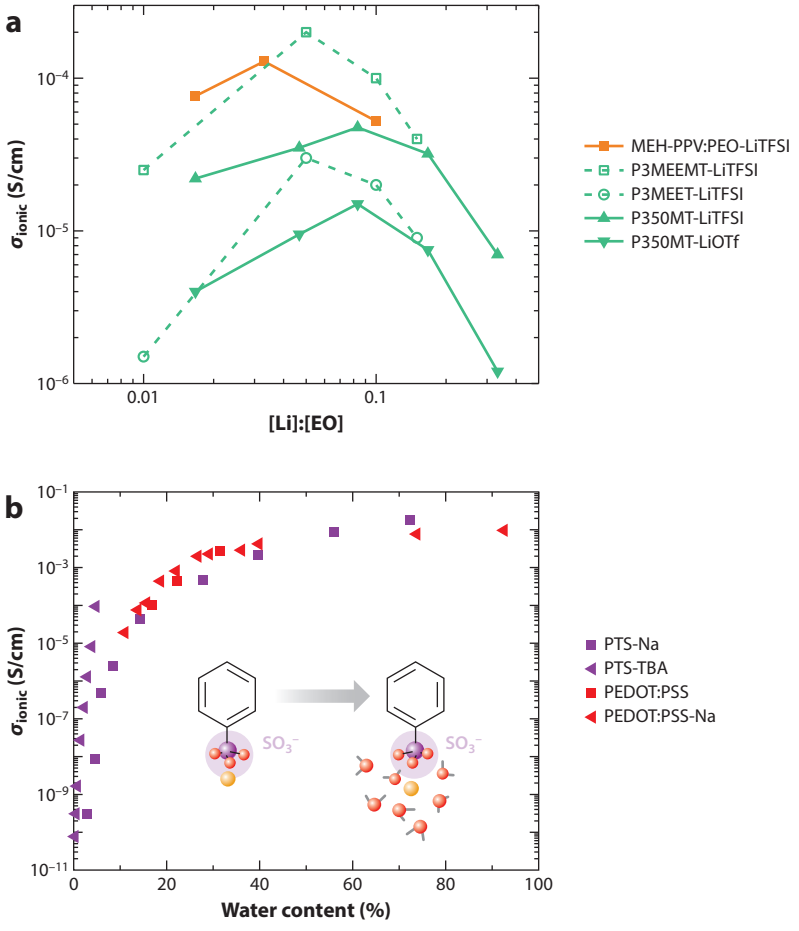

Figure 4

Ionic conductivity dependence on (*a*) cation concentration (cation per ether oxygen) in dry type II and VI polymer electrolyte–based MIECs and (*b*) water content in hydrated type I and V polyelectrolyte-based MIECs. Panel *a* highlights the general effect of ion-ion interactions limiting σ_{ionic} as the cation:ether oxygen ratio approaches 0.1. The inset in panel *b* illustrates the dissociative effect of hydration, which leads to dramatic increases in σ_{ionic}. Abbreviations: EO, ether oxygen; LiOTf, lithium trifluoromethanesulfonate; LiTFSI, lithium bis(trifluoromethane)sulfonimide; MEH-PPV, poly[2-methoxy-5-(2-ethylhexyloxy)-1,4-phenylenevinylene]; MIEC, mixed ionic-electronic conductor; P350MT, poly[3-oligo(oxyethylene)-4-methylthiophene]; P3MEEMT, poly[3-(methoxyethoxyethoxymethyl)thiophene]; P3MEET, poly[3-(methoxyethoxyethoxy)thiophene]; PEDOT, poly(3,4-ethylenedioxythiophene); PEO, poly(ethylene oxide); PSS, poly(styrene sulfonate); PTS, poly[6-(thiophen-3-yl)hexane-1-sulfonate]; TBA, tetrabutylammonium. Panel *b* adapted with permission from Reference 52; copyright 2020 American Chemical Society.

2.4.3. Electrolyte swollen ionic transport. Many applications require polymeric MIECs to be in contact with liquid electrolytes (10, 11, 14, 16). This complicates the description of transport, as ions and solvent are now in a concentration- and electrochemical potential–dependent equilibrium between the contacting liquid electrolyte and polymer MIEC (63). This is most obvious in potential-dependent swelling of polymeric MIECs in response to electrochemically induced electronic charge. In this environment, many marginal polymeric MIECs that

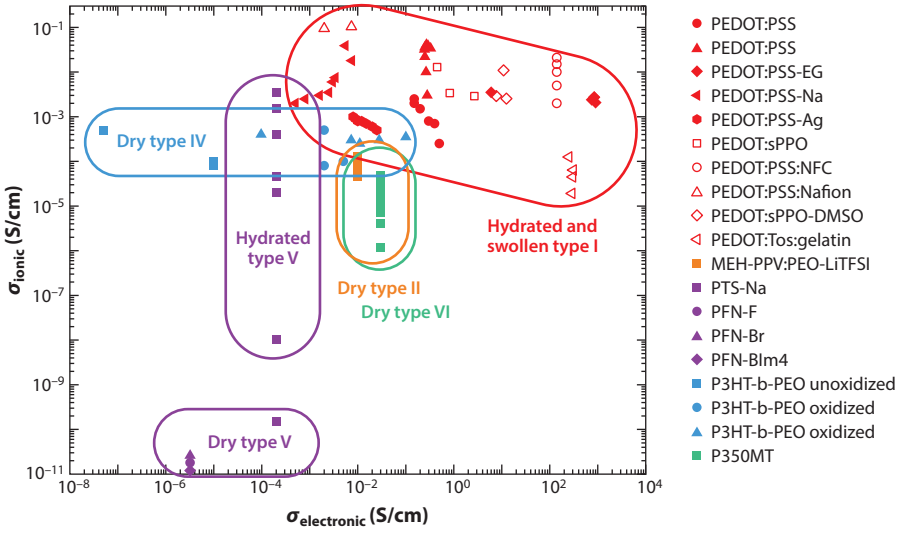

Figure 5

Ionic and electronic conductivity map of various types of polymeric mixed ionic-electronic conductors under dry, hydrated, electrolyte swollen, and gelled conditions. The degree of doping and hydration leads to a several orders of magnitude range of electronic and ionic conductivity, respectively. Dry polymer electrolyte-based materials (types II, IV, and VI) show much better ionic conductivity than dry polyelectrolyte-based materials (type V). However, hydrated and solvent swollen polyelectrolyte/conjugated polymer composites (type I) show both the best ionic and electronic conductivity. Abbreviations: BIm4, tetrakis(imidazolyl)borate; DMSO, dimethylsulfoxide; EG, ethylene glycol; LiTFSI, lithium bis(trifluoromethane)sulfonimide; MEH-PPV, poly[2-methoxy-5-(2-ethylhexyloxy)-1,4-phenylenevinylene]; NFC, nanofibrillated cellulose; P3HT, poly(3-hexylthiophene); P350MT, poly[3-oligo(oxyethylene)-4-methylthiophene]; PEDOT, poly(3,4-ethylenedioxythiophene); PEO, poly(ethylene oxide); PFN, poly[9,9′-bis[6″-(N,N,N-trimethylammonium)hexyl]fluorene-alt-co-phenylene]; PSS, poly(styrene sulfonate); sPPO, sulfonated poly(2,6-dimethyl 1,4-phenylene oxide); Tos, tosylate.

minimally solvate/transport ions become surprisingly effective mixed conductors. As an example, the type VI material poly(2-(3,3′-bis(2-(2-(2-methoxyethoxy)ethoxy)ethoxy)-[2,2′-bithiophen]-5-yl)thieno[3,2-b]thiophene) [p(g2T-TT)] passively swells only ∼10% when in contact with aqueous NaCl, independent of electrolyte concentration. However, upon the application of an oxidizing potential, p(g2T-TT) reversibly swells an additional 42% to 86% (63). This exemplifies the important contribution of electronic charge in ion solvation and coordination. In a similar material with roughly double the density of oligoethylene glycol side chains, the reversible swelling in response to electrochemical potential is increased to ∼300% and can exceed 1,000%, though irreversibly (64). This electrochemical potential–dependent polymeric MIEC swelling is intuitively expected to lead to large changes in σ_{ionic}, though this has yet to be directly experimentally verified.

In traditional hydrophobic CPs, electrochemical potential–dependent swelling manifests as voltage-switchable semiconductor to mixed conductor behavior. In the neutral state (absence of electronic charge), hydrophobic CPs do not dissolve ions or water; however, once electronic charge is present, it is energetically favorable (required) that dopant ions are present and thus the film swells with electrolytes. The electrochemical potential necessary for this to occur is not simply connected to the highest occupied molecular orbital (HOMO) level of the CP; it includes an ion-dependent overpotential (65) that increases with decreasing ion polarizability and is inversely proportional with ion miscibility in the CP (42). In true MIEC polymers that

are sufficiently able to solvate ions, this overpotential is effectively zero, and the onset of electrochemical potential–dependent swelling tracks with HOMO/lowest unoccupied molecular orbital (LUMO) level positions.

Peculiarly, the rigid backbone ladder (BBL) polymer (**Figure 1*d***) passively swells ∼10% when in contact with an aqueous electrolyte and swells ∼100% upon application of a reductive potential with little apparent overpotential (66). This is quite unexpected due to the low density of ion coordination sites (carbonyl groups), and the large ℓp of BBL (∼1,530 Å) (67) would imply the inability of local segmental motion to assist ionic transport. BBL may have sufficient free volume to allow ion and water penetration, and due to its rigidity it may form a unique rigid rod gel network, allowing a high degree of swelling; however, this phenomenon deserves further study.

As with highly hydrated systems, polyelectrolyte-based MIECs in contact with liquid electrolytes display facile ionic transport. Across a variety of ions, PEDOT:PSS σ_{ionic} shows the same concentration dependence as liquid electrolytes (68). PEDOT:PSS moving front experiments revealed ion mobilities on par with aqueous electrophoretic mobilities (69). As excessive swelling can be detrimental to device stability, cross-linkers are often employed to decrease polymeric MIEC swelling. In cross-linked PEDOT:PSS, the ionic mobility was decreased by an order of magnitude, in keeping with the expected swelling-conductivity relationship (69).

Type I polymeric MIECs incorporating proton-conducting ionomers in acidic electrolytes reach very high σ_{ionic} values (10^{-2}–10^{-1} S/cm) (**Figure 5**), almost assuredly due to Grotthuss transport of protons through a hydrogen-bonded network (70, 71). In PEDOT templated on sulfonated poly(2,6-dimethyl 1,4-phenylene oxide), the proton hopping activation energy in 1 M sulfuric acid (34–72 meV) was over 20 times lower than the activation energy of chain-dependent hopping in dry polyelectrolyte-based MIECs. Highlighting the effect of the Grotthuss mechanism, in the same material, Li^+ conductivity was one-tenth that of protons (71).

Many studies assume single ion transport between the MIEC and liquid electrolytes. Any additional mass transport has been ascribed to solvent transport. In the case of polyelectrolyte-based MIECs (types I, III, and V), this assumption is likely true, as Donnan exclusion arising from the fixed polyelectrolyte charge should prevent transport of ions of the same charge as the polyelectrolyte. However, in polymer electrolyte–based MIECs (types II, IV, and VI), there is neither fixed ionic charge nor Donnan exclusion. Both anions and cations are in equilibrium between the liquid electrolyte and the MIEC, and single ion transport is at odds with experimental observations of dopant and counterion uptake (72–74).

2.4.4. Hydrogel ionic transport. Both highly hydrated and electrolyte swollen polymeric MIECs are more accurately described as conductive hydrogels, which is an area of explicit research (75–78). In such hydrogels, ionic transport is decoupled from polymer chain dynamics, as continuous liquid pathways are available for ionic transport. Thus, engineering high σ_{ionic} is unnecessary; instead, maintaining a percolative path for effective electronic transport is the main design goal, as discussed in Section 3.6. Separately engineering the electronic transport pathways while maintaining liquid (void) spaces spanning the nano- to mesoscale leads to considerable overlap between MIEC hydrogels and structured porous materials (77).

3. ELECTRONIC TRANSPORT IN POLYMERIC MIXED IONIC-ELECTRONIC CONDUCTORS

Of the extensive body of work studying electronic transport in CPs, the most insightful parallels to transport in polymeric MIECs can be drawn from studies of molecular and electrochemically doped CPs. While molecular dopants ionize to donate an electronic charge, electrochemical

RADICAL POLYMERS

As the name suggests, radical polymers can stabilize electronic charge not through conjugation and delocalization, but through stable open-shell moieties, i.e., radicals. These radicals can couple with ions in a similar manner as electrochemical doping in CP-based MIECs (73), and their mixed conducting properties have made them attractive materials for battery electrodes (79). Ionic transport occurs in the same chain motion–dependent manner as traditional polymer electrolytes. Radicals are often localized to pendant groups, and electronic transport occurs through self-exchange between pendant groups that are brought into close proximity via chain motion (80). In contrast to CPs, radical polymers do not require a rigid backbone for electronic transport. Instead, the same chain motion that imparts ionic conductivity also imparts electronic conductivity, with both showing a strong dependence on T_g (81).

dopants are ions and tend to electrostatically stabilize electronic charge. Though both can occur in polymeric MIECs, electrochemical doping is especially important to consider due to the high ion concentrations present. While the focus on CP-based systems reflects the state of the field, not all polymer MIECs are conjugated (see the sidebar titled Radical Polymers).

3.1. The Nature of Electronic Carriers

Just as ionic transport in polymeric MIECs requires the appropriate chemical functionality to solvate ions, electronic transport requires the proper electronic structure to stabilize mobile electronic charge carriers. This requisite electronic structure is most commonly achieved through extended conjugation that creates delocalized π-orbitals. Electronic carriers can be induced by adding an electron (reduction) or removing an electron to create a positively charged hole (oxidation). Following the nomenclature of semiconductors, polymeric MIECs that are readily oxidized and reduced are referred to as p- and n-type materials, respectively, while those that undergo both are referred to as ambipolar.

While anions and cations in close proximity can form neutral pairs, unless the energetics are precisely engineered (82), an electron and hole in close proximity tend to recombine, annihilating both. Thus, it is unlikely to have areas of both sustained electron and hole concentration. Instead, recombination zones form at the interface of n- and p-type regions, as exploited in LEECs (32).

The relative ease with which an electronic carrier can be induced by molecular or electrochemical doping is directly related to the polymeric MIEC molecular orbitals' energy level positions. To induce an electron, the LUMO must be sufficiently deep, or to induce a hole, the HOMO must be sufficiently shallow to be within accessible potentials for the given electrolyte system. For systems containing water, this range is ∼4.0 to ∼5.4 eV deep on the vacuum scale (83, 84).

Unlike crystalline inorganic materials in which electronic charge carriers are nearly completely delocalized and interact little with the materials crystalline lattice, electronic carriers in polymeric MIECs are closely coupled to local structural deformations. It is useful to treat the electronic charge and coupled lattice deformation as a single quasiparticle termed a polaron. Polarons themselves can combine into large quasiparticles to form bipolarons and multipolaronic/bipolaronic species (85).

Electroneutrality dictates that oppositely charged ions balance electronic carriers. The fixed polyelectrolyte charge in type I/III/V materials can serve this function, while type II/IV/VI materials require the injection of counterbalancing dopant anions or cations. Alternatively, electronic carriers can be introduced into polymeric MIECs through molecular doping with molecules that favorably undergo charge transfer with polymeric MIECs. The same chemical functionality

that allows polymeric MIECs to solvate ions has also been found to improve molecular doping efficiency (86, 87).

3.2. Mechanism of Electronic Transport

As with ions, electrons and holes move in response to applied field and concentration gradients. The drift-diffusion equation in one dimension gives the current density (J_n) for electrons,

$$J_n = en\mu_n \frac{d\phi}{dx} + eD_n \frac{dn}{dx},$$

and the current density (J_p) for holes,

$$J_p = ep\mu_p \frac{d\phi}{dx} - eD_p \frac{dp}{dx},$$

where n and p are the number densities, μ_n and μ_p are mobilities, and D_n and D_p are the diffusivities for the electrons and holes, respectively. Thus, the n- and p-type electrical conductivities are given as $\sigma_n = en\mu_n$ and $\sigma_p = ep\mu_p$, respectively. Absent molecular doping, n and p are equal to the excess cation and anion concentrations, respectively. This is especially relevant in polymeric MIECs that are coupled with an external electrolyte and are under potentiostatic control.

Electronic charge transport in doped CPs is often described as Efros–Shklovskii variable-range hopping (28, 88, 89), in which the electronic conductivity ($\sigma_{electronic}$) has the following temperature dependence:

$$\sigma_{electronic} = \sigma_{ES} e^{\left(\frac{T_{ES}}{T}\right)^{-\frac{1}{2}}},$$

where σ_{ES} is the conductivity prefactor and T_{ES} is the characteristic temperature. The fundamental insight of this model is the presence of a Coulomb gap in the density of states (DOS) at the Fermi level. The Coulomb gap can be qualitatively rationalized as the energetic distance between the highest filled localized states (Fermi level) and the lowest empty delocalized states (transport level or mobility edge) (see inset in **Figure 6*a***). Increasing the charge density should decrease T_{ES} such that at or above T_{ES}, the thermal energy should be sufficient to collapse the Coulomb gap, resulting in high (metallic) conductivity (28). However, this has not been unequivocally achieved (90), likely due to dopant-induced disorder that accompanies high carrier densities (28).

Over smaller temperature ranges, electronic mobility is commonly (if not strictly accurately) described as thermally activated hopping with an Arrhenius relationship:

$$\mu = \mu_0 e^{\left(\frac{-E_a}{RT}\right)},$$

where the activation energy (E_a) and exponential prefactor (μ_0) are carrier density dependent. The activation energy is a useful parameter to approximate the difference between the Fermi level and transport level to compare the mobility at different carrier densities and in different materials (91, 92).

Efficient electronic transport in polymeric MIECs depends on particular characteristics on different length scales. On the shortest length scale, the degree of carrier localization is paramount. Decreased localization leads to lower activation energies and higher mobilities. Localization depends intrinsically on the chemical and molecular structure and extrinsically on the proximity of ions. Carriers can be localized to a particular repeat subunit due to its electron-accepting or -donating character. Alternatively, large dihedral angles between repeat units can limit delocalization of charge to single (or few) repeat units. A classic CP example is regiorandom P3HT, in which

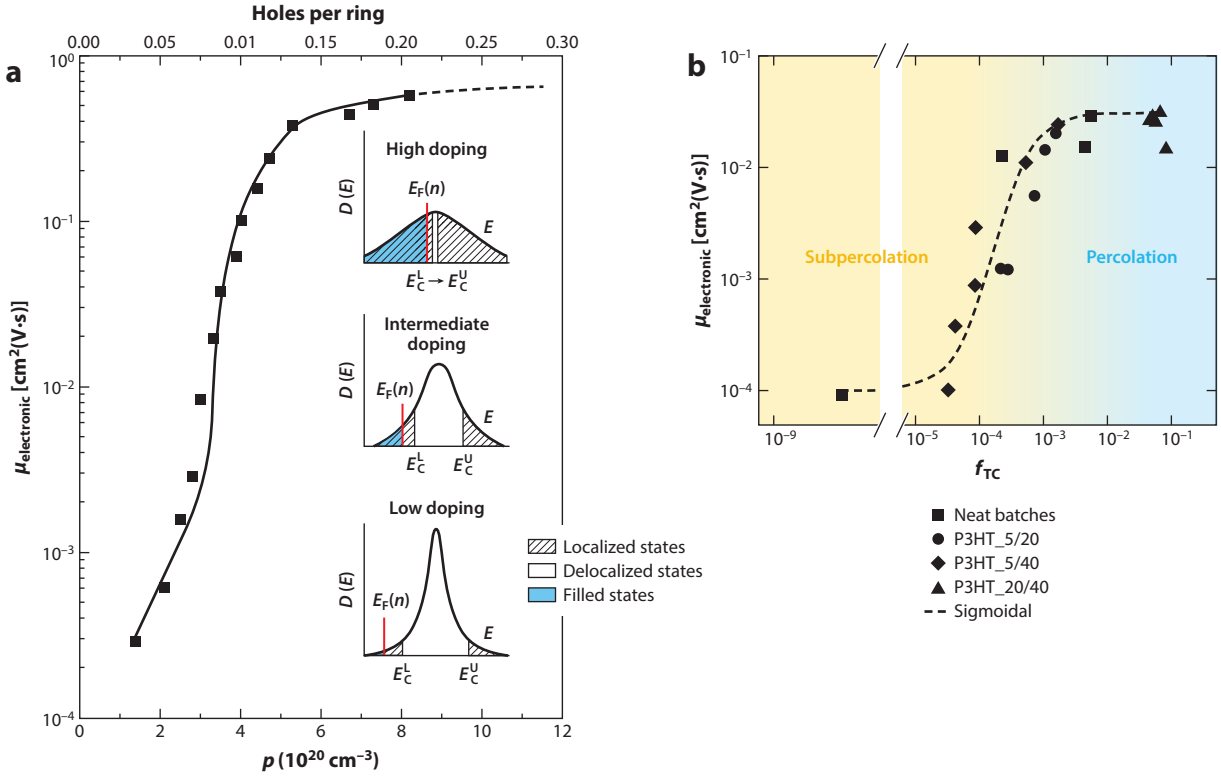

Figure 6

Electronic charge transport in the prototypical conjugated polymer (CP) system poly(3-hexylthiophene) (P3HT): (*a*) doping-dependent electronic mobility showing the dramatic rise and plateau with increased ionic dopant concentration (*p*) and (*b*) tie chain–dependent mobility in the prototypical CP P3HT, demonstrating the critical fraction of tie chains (f_{TC}) necessary for efficient electronic charge transport through a percolated network. The insets in panel *a* show the density of states (*D*) filled up to the Fermi level (E_F) and the transport level (E_C), where the difference between E_F and E_C is the activation energy. E_C^L and E_C^U are the lower and upper transport levels, respectively. The broadening of the density of states distribution with increased doping drives the localization of states and shifts E_C, which frustrates the transition to true band-like or metallic transport. Panel *a* adapted from Reference 28; copyright 2012 Macmillan Publishers. Panel *b* adapted from Reference 102; copyright 2018 American Chemical Society.

the steric hindrance of side chains in head-to-head coupled thiophenes introduces significant torsion, decreasing the conjugation length and localizing charge, which widens the optical bandgap and decreases $\sigma_{electronic}$ (93, 94). In comparison, all head-to-tail coupled regioregular P3HT lacks this torsion and shows charge delocalization over 10 repeat units (95). This is reflected in the ℓp of regiorandom (~10 Å) and regioregular (~29 Å) P3HT (36). When localization is the limiting factor, it leads to mixed valence redox transport in which $\sigma_{electronic}$ maximums are observed in the half-charged states (96). However, in most polymeric MIECs, localization is not so extreme and is one of several factors that affect electronic transport.

On longer length scales, intrachain, interchain, and interdomain transport sum to produce macroscopic percolated electronic transport pathways. Low disorder (low torsion) that decreases carrier localization also improves transport down the chain backbone (intrachain transport). Planarity can be enhanced by backbone design or through intermolecular interactions (aggregation or crystallinity). Inherently planar backbones with fused rings or chemical functionality that limit torsion at single bond linkages (e.g., BBL, ℓp ~1,530 Å) display low energetic disorder,

independent of molecular packing (67, 97). In aggregates and crystallites, intermolecular interactions can force otherwise somewhat flexible chains into more ordered extended planar structures, more than doubling their ℓp values (37) and extending charge carrier delocalization along the chain and onto neighboring chains (98), allowing efficient interchain transport. The extent of ordering can be just a few chains aggregated together up to crystallites hundreds of nanometers in diameter, with increased aggregation or crystallinity generally correlated with improved electronic transport. Within the limit of very rigid planar polymers, the minimum requisite aggregation for efficient interchain transport can be single close contacts between two chains (99).

The intermolecular aggregation or crystallinity that allows efficient interchain transport also produces discrete boundaries between crystallites and between crystalline and amorphous domains. Interdomain transport is impeded by the boundaries themselves and the high disorder of the amorphous regions (90). Doped CPs that show completely delocalized (metallic) carriers in ordered domains still display thermally activated macroscopic transport due to these boundaries and amorphous regions (89). The effect of boundaries is minimized in films of highly rigid chains or aligned domains in which boundaries are gradual and low angle (99, 100). Still, traversing the amorphous regions between crystallites requires individual connecting tie chains between crystallites or aggregates (**Figure 6*b***), resulting in a positive correlation between electronic transport and molecular weight, as longer chains more often bridge crystallites (101, 102). This is exemplified in oligomeric MIECs that show much lower $\sigma_{electronic}$ than similar polymeric analogs (103, 104).

3.3. Effect of Ions on Electronic Transport

Ions complicate electronic transport. At low concentrations, ions present deep Coulomb wells that localize (trap) carriers and decrease their mobility (**Figure 6*a***) (94, 105, 106), such that the carrier mobility in electrochemically doped devices is over an order of magnitude lower than that in field effect devices at equivalent volumetric charge carrier density (91). Above ~0.1% doping (1 dopant ion per 1,000 repeat units), electronic mobilities dramatically increase with increased dopant concentration as the tail of the DOS fills (**Figure 6*a***) (106), and Coulomb wells overlap, smoothing the energy landscape and reducing the hopping activation energy (92). This is reflected in an increased dielectric constant screening ions and carriers and increased carrier localization lengths (28). High doping levels (~10%) lead to high mobilities [0.1–10 $cm^2/(V{\cdot}s)$] and $\sigma_{electronic}$ (10–1,000 S/cm) (88, 92, 107, 108), with hopping activation energies equivalent to the thermal energy (k_bT) at room temperature (91, 92). Above 10% doping, $\sigma_{electronic}$ improvements diminish, with mobility plateauing as the cumulative disorder that accompanies doping flattens the DOS and decreases the number of delocalized transport states (see inset in **Figure 6*a***) (28). At extreme doping levels, disorder is so great that carrier mobility is suppressed and $\sigma_{electronic}$ is extinguished (92).

3.4. Dry Electronic Transport

In dry type V materials, while total ion concentrations are high, the dopant concentration (excess anion or cation) is well below 1% (51), and carrier mobility is quite low [$\sim 10^{-5}$ $cm^2/(V{\cdot}s)$] (**Figure 5**) (109). Type IV materials with balanced anion and cation concentrations also show quite low $\sigma_{electronic}$ (10^{-8}–10^{-7} S/cm) (**Figure 5**) but can be increased approximately five orders of magnitude by introducing excess dopant anions. Further, the dopant-conductivity relationship is not simply linear, as a 10-fold increase in dopants yields a 100-fold increase in $\sigma_{electronic}$ (110). PEDOT:PSS (type I) is inherently highly doped (~30%) by the PSS^- on which it is templated. Additives or processing that remove superfluous PSS, improve domain purity, and create a well-percolated network of PEDOT-rich domains yield $\sigma_{electronic}$ > 1,000 S/cm (**Figure 5**) (88, 107, 111).

3.5. Hydrated and Electrolyte Swollen Electronic Transport

In undoped CPs, water acts as an electronic trap, diminishing electronic transport, and the displacement of water molecules from CP films drastically improves the electronic properties (112). Polymeric MIECs' high carrier densities can saturate such traps, and their coordinating groups can potentially interact with water without creating traps, as they display high $\sigma_{electronic}$ in aqueous environments. The intrinsic and molecular doped $\sigma_{electronic}$ of conjugated polyelectrolytes (type V) is relatively insensitive to hydration (41, 52, 60). Similarly, high $\sigma_{electronic}$ formulations of PEDOT:PSS (type I) are insensitive to hydration (60), while low $\sigma_{electronic}$ formulations show only a factor of 3 decrease in $\sigma_{electronic}$ at 100% RH (59).

When polymeric MIECs are in contact with a liquid electrolyte, the dopant density is directly tunable with electrochemical potential, making them prime channel materials for organic electrochemical transistors (11, 113–116). The massive change in $\sigma_{electronic}$ with charge density permits high transconductance (gain), quantified by the intrinsic material figure of merit μC^*, the product of the charge carrier mobility and volumetric capacitance (reflecting the DOS) (117, 118).

The equilibrium between polymeric MIECs and liquid electrolytes leads to a strong dopant density dependence on electrolyte concentration and pH, in addition to electrochemical potential (63, 119, 120). The $\sigma_{electronic}$ of PEDOT:PSS is enhanced in acidic conditions, while increasing the pH decreases doping and increases in cation exchange, with sodium cations supplanting protons and preferentially associating with PSS^- (at the expense of holes on PEDOT) (121). This is reflected in PEDOT templated on poly(4-styrenesulfonic acid) sodium salt (PSSNa), which displays quite low $\sigma_{electronic}$ that is very sensitive to hydration (52, 60).

Interdomain transport can be physically disrupted by the swelling that accompanies hydration and electrolyte exposure (52, 63, 64, 122). Monitoring crystallinity with in situ and ex situ X-ray scattering indicates that the bulk of the swelling must occur in the amorphous domains (26, 63, 123). Electronic transport should be especially sensitive to tie chains or domain contacts that create percolated pathways (**Figure 6*b***). In CP electrolytes (type VI), some swelling is necessary to facilitate dopant ion injection, but excessive swelling leads to decreases in carrier mobility (124–126).

3.6. Hydrogel Electronic Transport

When highly swollen, polymer MIECs are functionally hydrogels. Typically, $\sigma_{electronic}$ is low, such that $\sigma_{electronic}$ approaching 10 S/cm is considered ultrahigh (77, 127–129), reflecting the loss of percolation with swelling. $\sigma_{electronic}$ is inversely proportional to the degree of swelling in both PEDOT:PSS poly(ethylene glycol)/poly(acrylic acid) double-network and PEDOT:PSS single-component hydrogels (78, 130). Ions further disrupt percolation (likely screening electrostatic interactions between aggregates), as gelation with phosphate-buffered saline reduces $\sigma_{electronic}$ by 50% compared to gelation with water (78). Rheological analysis is common to hydrogel characterization (129), and given the expected connections between the percolated electronic and mechanical networks, combined rheological and electrical analysis is a promising avenue of study (131).

4. IONIC VERSUS ELECTRONIC TRANSPORT

On the surface, the structural characteristics of efficient electronic transport (rigid chains, semicrystalline structure) seem at odds with characteristics of efficient ionic transport (flexible chains, amorphous structure). This holds true for homogenous polymeric MIECs (types V and VI), in which the same backbone must impart electronic and ionic transporting characteristics and mixed transport requires a compromise of individual ionic and electronic transport

(41, 49, 52, 132). Further, swelling that increases ionic transport strains the percolated pathway of electronic transport. However, such compromises are largely sidestepped by separating the ionic and electronic transport into separate domains (types I, II, III, and IV). Dry type IV block copolymers show independently tuned ionic (via salt concentration) and electronic (via degree of oxidation) transport (**Figure 5**) (40, 47). Control of PEDOT:PSS (type IV) morphology and hydration allows simultaneous high ionic and electronic conductivity (60, 61, 69, 71), with a 100-fold increase in electronic conductivity diminishing ion diffusivities by a factor of only two (107). For context, it is worth remembering that some of the highest electrical conductivities in polymers occur in mixed conducting materials (88, 111). Further, simply maximizing both is not the universal goal in polymer MIEC-based applications; instead, it is the rational control of ionic and electronic transport. For instance, increased ionic transport leads to faster response times in LEECs (58); conversely, decreased ionic transport leads to faster response times in organic light-emitting diodes (133), and restraining ionic transport imparts nonvolatility in synaptic-like devices (134). Given the wide variety of polymeric MIECs, there is likely to be a proper balance of mixed conducting properties to satisfy most applications.

5. HEAT AND ENERGY TRANSPORT IN POLYMERIC MIXED IONIC-ELECTRONIC CONDUCTORS

In addition to drift and diffusion, thermal gradients drive the transport (thermodiffusion) of both ionic and electronic charges. Moreover, mobile charge opens additional routes for heat transport. Thus, polymeric MIECs show unique thermodiffusion and thermal transport compared to pure electronically or ionically conducting polymers.

5.1. Seebeck Coefficient

An applied thermal gradient (ΔT) drives thermodiffusion of charge carriers from the hot to the cold (high to low entropy) ends, establishing a steady-state thermovoltage (ΔV). Known as the Seebeck effect, the proportionality constant between ΔV and ΔT is the Seebeck coefficient ($S = -\Delta V/\Delta T$). Also known as thermopower, S is the entropy transported by a carrier divided by its charge and represents a sum of contributions of the different charge carriers and their transport. For predominantly electronic conductors (e.g., PEDOT:tosylate), ΔV increases with increasing ΔT until saturating at a few tens or hundreds of microvolts per Kelvin (97, 136, 137). Electronic carriers thermodiffuse quickly, and the response of ΔV to ΔT is relatively fast (**Figure 7*a***) (138). Conversely, in pure ionic conductors (e.g., PSSNa), ΔV is slow to reach steady state as ions thermodiffuse slowly due to the Soret effect. If only cations are mobile, as in the case of PSSNa, they will thermodiffuse faster than the immobile anions, accumulating at the cold end of the electrode. The resulting positive ΔV ($\sim$10 mV/K) is 1,000$\times$ that of pure electronic conductors (139–141) and varies with ambient RH (60), as hydration enhances the thermodiffusion of the cations (**Figure 7*a***).

In polymeric MIECs (e.g., PEDOT:PSS), the evolution of ΔV with ΔT is the result of two competing effects: ionic versus electronic thermodiffusion. Initially, cations accumulate at the cold end, and ΔV increases steadily as ΔT increases, reaching a maximum value of 0.1–1 mV/K depending on RH. This ionic transport changes the doping level locally throughout the sample (138), causing electronic and ionic carriers to redistribute to ensure electroneutrality. This is accompanied by a decrease in ΔV to $\sim$5–10 μV/K, equivalent to the pure electronic contribution to ΔV (**Figure 7*a***). Unlike the ionic contribution, the electronic contribution to ΔV is independent of the relative humidity (60). Because of its transient nature, this ionic Seebeck effect in MIECs

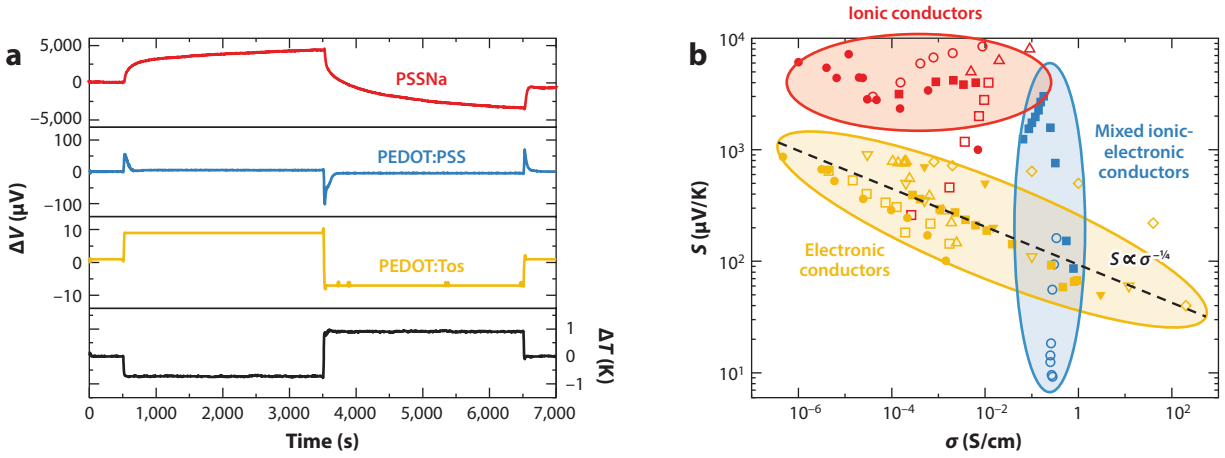

Figure 7

(*a*) Evolution of thermovoltage with time for a typical electronic conductor (PEDOT:Tos), an ionic conductor (PSSNa), and a mixed ionic-electronic conductor (PEDOT:PSS) at 80% relative humidity. (*b*) Seebeck coefficient versus electrical conductivity for electronic conductors (*yellow*), ionic conductors (*red*), and mixed ionic-electronic conductors (*blue*). The empirical trend $S \propto \sigma_{electronic}^{-1/4}$ observed for electronic conductors is shown for reference. Abbreviations: PEDOT, poly(3,4-ethylenedioxythiophene); PSS, poly(styrene sulfonate); PSSNa, poly(sodium 4-styrenesulfonate); Tos, tosylate. Panel *a* adapted with permission from Reference 138; copyright 2016 Wiley-VCH Verlag. Panel *b* adapted with permission from Reference 135; copyright 2020 Wiley-VCH Verlag.

does not contribute to power generation, but it can be exploited for simultaneous independent pressure-humidity-temperature sensing (141).

Mobile electrochemically active redox species and reactive electrodes allow continual thermogenerated ionic currents and constant power generation in polymeric MIECs. Ag^+ electrochemically reacting with silver metal electrodes in PEDOT:Ag:PSS gives rise to a thermogalvanic effect (59). Holes are transported in the PEDOT-rich regions, while cations (Ag^+ and/or protons) thermodiffuse preferentially within the PSS-rich domains, generating an extra constant current on top of the nonconstant ionic Seebeck effect. The addition of pure ionic conductors like PSSH to polymeric MIECs results in hydrogels that are able to maintain the hydration necessary for effective ionic transport under ambient conditions, yielding stable thermopowers >15 mV/K (142). The sign of the Seebeck coefficient can also be reversed from positive (mobile cations) to negative (mobile anions) by tailoring the ion/polymer matrix interaction (143, 144).

S and $\sigma_{electronic}$ of pure electronic conductors are interrelated as a function of the charge carrier concentration (i.e., S decreases as σ increases). This behavior is typically rationalized in terms of the energy of the carrier with respect to the chemical potential of the material. Upon doping, an increase in charge carrier concentration drives the Fermi level closer to the transport level, such that the energy per carrier decreases. An empirical power law relationship between S and $\sigma_{electronic}$ (i.e., $S \propto \sigma_{electronic}^{-1/4}$) has been observed across a broad range of $\sigma_{electronic}$ for different pure electronic conductors (**Figure 7*b***) (145). While the origin of this quasiuniversal trend is yet to be understood, it is typically attributed to inhomogeneity in the polymeric film morphology (146) or to energetic disorder due to the presence of ionized dopants (147). Structural anisotropy in crystalline polymers can induce both S and $\sigma_{electronic}$ to increase simultaneously (148), yielding power factor values ($S\sigma^2$) that go beyond those predicted by the empirical power law relationship.

Polymeric pure ionic conductors do not typically follow this quasiuniversal trend (**Figure 7*b***). In polymeric ion gels, the σ_{ionic} increases with increasing ionic liquid content, while the ionic

Seebeck coefficient remains constant (143). In PSS, increased hydration increases the cation mobility (anions are immobile in PSS), without varying the ion concentration (149), simultaneously increasing both S and σ_{ionic}, leading to an S versus σ relationship orthogonal to that of pure electronic conductors. A similar trend was reported for polymeric MIECs, in which conductivity is primarily dominated by humidity-independent electronic transport, while the Seebeck coefficient is largely dominated by humidity-dependent ionic thermodiffusion (**Figure 7*b***) (60).

5.2. Thermal Conductivity

In electronic conductors, phonons and electrons contribute to heat transport, and the resulting thermal conductivity (κ) has a lattice (κ_L) and electronic (κ_{el}) component, such that $\kappa = \kappa_L + \kappa_{el}$. κ_{el} and $\sigma_{electronic}$ are related by the Wiedemann-Franz law, $\kappa_{el} = LT\sigma_{electronic}$, where L is the Lorentz number. In CPs, κ_{el} is typically 0.1–0.5 W/(m·K), with κ_{el} becoming significant when $\sigma_{electronic}$ exceeds 10 S/cm (151). As heat transport is more efficient through covalent bonding along the chain direction than through van der Waals interactions between chains, amorphous and ordered regions have different contributions to κ. In PEDOT:PSS, anisotropic phase separation results in anisotropic κ (152), with fast in-plane heat transport through interconnected (high $\sigma_{electronic}$) PEDOT-rich domains and slower PSS-limited heat transport out of plane (**Figure 8*a***) (153). This anisotropy vanishes with increased PSS loading, and κ approaches that of pure PSS as in-plane $\sigma_{electronic}$ decreases and heat transport is limited by PSS in all directions (**Figure 8*b***) (150).

Polyelectrolytes display a hydration-dependent κ. In PSSNa, κ increases from 0.35 to 0.49 W/(m·K), when RH is increased from 50% to 100% (149). This rise is explained as the formation of parallel polymer-rich and aqueous-rich paths of thermal transport [κ_{H2O} = 0.6 W/(m·K) at room temperature]. Similar trends are reasonably expected in hydrated polymeric MIECs. Hydration should affect κ_L but not κ_{el}, as $\sigma_{electronic}$ is independent of hydration and σ_{ionic} is typically less than 10^{-2} S/cm (60). To a first approximation, the thermal conductivity should be a composition-weighted average of the lattice contributions to the thermal conductivity of the solvent and of the conducting polymer. However, the empirical results are more complicated

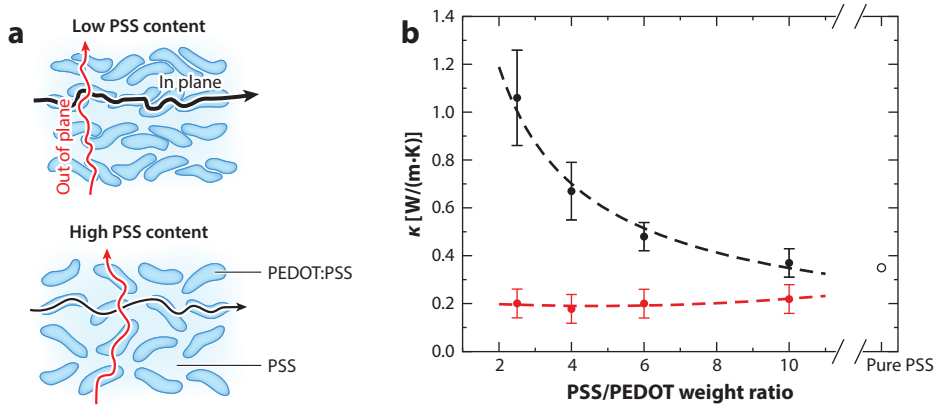

Figure 8

(*a*) Similar to charge transport, heat transport in PEDOT:PSS is fast along the in-plane direction and slow in the out-of-plane direction. (*b*) In-plane (*black*) and out-of-plane (*red*) thermal conductivity versus PSS load (value of κ for PSS taken from Reference 149). Abbreviations: PEDOT, poly(3,4-ethylenedioxythiophene); PSS, poly(styrene sulfonate). Figure adapted with permission from Reference 150; copyright 2019 Wiley-VCH Verlag.

with high and low $\sigma_{electronic}$ PEDOT:PSS showing opposite trends in κ with hydration (154). This complex behavior calls for a better understanding of thermal transport in polymeric MIECs.

6. CONCLUSION

There is a growing body of work studying mixed ionic and electronic transport in polymeric materials. Mixed ionic and electronic transport in polymers requires proper chemical functionality to solvate ions and stabilize electrons and/or holes. Ionic transport depends on chain motion, while electronic transport depends on intermolecular interactions and macroscopic percolation. This can be achieved with a variety of polymer blends, block copolymers, and homopolymers, each with their own strengths and weaknesses. The varied applications of polymeric MIECs require vastly different operating environments (dry, hydrated, electrolyte swollen, etc.), which leads to the same material displaying drastically different mixed conducting properties depending on environment. However, proper choice of polymer MIECs can provide efficient mixed transport irrespective of application environment. Studies thus far have focused on a limited range of materials (mostly PEDOT:PSS based), and quantitative reports of ionic transport are for the most part limited to type I and IV polymeric MIECs. Expansion of ionic transport studies to a wider range of polymeric MIECs is needed. Investigations of additives for increased ionic transport in dry materials are currently lacking. Low disorder planar CP electrolytes and polyelectrolytes have tantalizing potential for improved electronic charge transport. Polymeric MIECs are uniquely capable of simultaneously containing and transporting very high ionic and electronic charge carrier densities, and the coupling between these high ionic and electronic charge densities lies at the heart of their unique functionality. Better understanding of these ionic-electronic coupling properties is the key to advancing new applications. Interest in polymeric MIECs is spread across many fields, and improving mixed transport in particular polymeric MIEC types and applications requires leveraging the collective knowledge across disciplines. Further progress across these fronts will improve the feasibility of polymeric MIECs in the many current areas of interest and open new application areas for these exciting materials.

DISCLOSURE STATEMENT

The authors are not aware of any affiliations, memberships, funding, or financial holdings that might be perceived as affecting the objectivity of this review.

ACKNOWLEDGMENTS

S.F. gratefully acknowledges support from the Swedish Research Council (2016–03979), Olle Engkvists Stiftelse (204–0256), and the Advanced Functional Materials Center at Linköping University (2009–00971). B.D.P. and J.R. gratefully acknowledge support from National Science Foundation grant NSF DMR-1751308. J.R. gratefully acknowledges support from the Alfred P. Sloan Foundation.

LITERATURE CITED

1. Bolto BA, McNeill R, Weiss DE. 1963. Electronic conduction in polymers. III. Electronic properties of polypyrrole. *Aust. J. Chem.* 16(6):1090–103
2. Shirakawa H, Louis EJ, MacDiarmid AG, Chiang CK, Heeger AJ. 1977. Synthesis of electrically conducting organic polymers: halogen derivatives of polyacetylene, $(CH)_x$. *J. Chem. Soc. Chem. Commun.* 1977(16):578–80

3. Fenton DE, Parker JM, Wright PV. 1973. Complexes of alkali metal ions with poly(ethylene oxide). *Polymer* 14(11):589
4. Wright PV. 1975. Electrical conductivity in ionic complexes of poly(ethylene oxide). *Br. Polym. J.* 7(5):319–27
5. Minett MG, Owen JR. 1988. Polymeric insertion electrodes. *Solid State Ion.* 28–30:1192–96
6. Paulsen BD, Tybrandt K, Stavrinidou E, Rivnay J. 2020. Organic mixed ionic-electronic conductors. *Nat. Mater.* 19(1):13–26
7. Costa RD, ed. 2017. *Light-Emitting Electrochemical Cells: Concepts, Advances and Challenges*. Cham, Switz.: Springer Int. Publ.
8. Melling D, Martinez JG, Jager EWH. 2019. Conjugated polymer actuators and devices: progress and opportunities. *Adv. Mater.* 31(22):1808210
9. van de Burgt Y, Melianas A, Keene ST, Malliaras G, Salleo A. 2018. Organic electronics for neuromorphic computing. *Nat. Electron.* 1(7):386–97
10. Zeglio E, Rutz AL, Winkler TE, Malliaras GG, Herland A. 2019. Conjugated polymers for assessing and controlling biological functions. *Adv. Mater.* 31(22):1806712
11. Rivnay J, Inal S, Salleo A, Owens RM, Berggren M, Malliaras GG. 2018. Organic electrochemical transistors. *Nat. Rev. Mater.* 3(2):17086
12. Sjöström TA, Berggren M, Gabrielsson EO, Janson P, Poxson DJ, et al. 2018. A decade of iontronic delivery devices. *Adv. Mater. Technol.* 3(5):1700360
13. Peterson KA, Thomas EM, Chabinyc ML. 2020. Thermoelectric properties of semiconducting polymers. *Annu. Rev. Mater. Res.* 50:551–74
14. Meng Q, Cai K, Chen Y, Chen L. 2017. Research progress on conducting polymer based supercapacitor electrode materials. *Nano Energy* 36:268–85
15. Xie J, Gu P, Zhang Q. 2017. Nanostructured conjugated polymers: toward high-performance organic electrodes for rechargeable batteries. *ACS Energy Lett.* 2(9):1985–96
16. Neo WT, Ye Q, Chua S-J, Xu J. 2016. Conjugated polymer-based electrochromics: materials, device fabrication and application prospects. *J. Mater. Chem. C* 4(31):7364–76
17. Ratner MA, Shriver DF. 1988. Ion transport in solvent-free polymers. *Chem. Rev.* 88(1):109–24
18. Bruce PG, ed. 1994. *Solid State Electrochemistry*. Cambridge, UK: Cambridge Univ. Press
19. Hallinan DT, Balsara NP. 2013. Polymer electrolytes. *Annu. Rev. Mater. Res.* 43:503–25
20. Choo Y, Halat DM, Villaluenga I, Timachova K, Balsara NP. 2020. Diffusion and migration in polymer electrolytes. *Prog. Polym. Sci.* 103:101220
21. Pace G, Friend R. 2013. Optical processes in conjugated polyelectrolytes dependence on chain conformation and film morphology. In *Conjugated Polyelectrolytes: Fundamentals and Applications*, ed. B Liu, GC Bazan, pp. 389–410. Weinheim, Ger.: Wiley-VCH Verlag
22. Mai C-K, Schlitz RA, Su GM, Spitzer D, Wang X, et al. 2014. Side-chain effects on the conductivity, morphology, and thermoelectric properties of self-doped narrow-band-gap conjugated polyelectrolytes. *J. Am. Chem. Soc.* 136(39):13478–81
23. Kee S, Haque MA, Lee Y, Nguyen TL, Rosas Villalva D, et al. 2020. A highly conductive conjugated polyelectrolyte for flexible organic thermoelectrics. *ACS Appl. Energy Mater.* 3(9):8667–75
24. Chevrier M, Kesters J, Houston JE, Van den Brande N, Chambon S, et al. 2021. Phosphonium-based polythiophene conjugated polyelectrolytes with different surfactant counterions: thermal properties, self-assembly and photovoltaic performances. *Polym. Int.* 70:457–66
25. Thomas EM, Brady MA, Nakayama H, Popere BC, Segalman RA, Chabinyc ML. 2018. X-ray scattering reveals ion-induced microstructural changes during electrochemical gating of poly(3-hexylthiophene). *Adv. Funct. Mater.* 28(44):1803687
26. Bischak CG, Flagg LQ, Yan K, Rehman T, Davies DW, et al. 2020. A reversible structural phase transition by electrochemically-driven ion injection into a conjugated polymer. *J. Am. Chem. Soc.* 142(16):7434–42
27. Matta M, Wu R, Paulsen BD, Petty AJ II, Sheelamanthula R, et al. 2020. Ion coordination and chelation in a glycolated polymer semiconductor: molecular dynamics and X-ray fluorescence study. *Chem. Mater.* 32(17):7301–8

28. Wang S, Ha M, Manno M, Frisbie CD, Leighton C. 2012. Hopping transport and the Hall effect near the insulator-metal transition in electrochemically gated poly(3-hexylthiophene) transistors. *Nat. Commun.* 3(1):1210
29. Volkov AV, Wijeratne K, Mitraka E, Ail U, Zhao D, et al. 2017. Understanding the capacitance of PEDOT:PSS. *Adv. Funct. Mater.* 27(28):1700329
30. Tybrandt K, Zozoulenko IV, Berggren M. 2017. Chemical potential-electric double layer coupling in conjugated polymer-polyelectrolyte blends. *Sci. Adv.* 3(12):eaao3659
31. Riess I. 2000. Polymeric mixed ionic electronic conductors. *Solid State Ionics* 136–137(1–2):1119–30
32. van Reenen S, Kemerink M. 2017. Light-emitting electrochemical cells: mechanisms and formal description. In *Light-Emitting Electrochemical Cells: Concepts, Advances and Challenges*, ed. RD Costa, pp. 3–45. Cham, Switz.: Springer Int. Publ.
33. Hiemenz PC, Lodge TP. 2007. *Polymer Chemistry*. Boca Raton, FL: CRC Press. 2nd ed.
34. Lee H, Venable RM, MacKerell AD, Pastor RW. 2008. Molecular dynamics studies of polyethylene oxide and polyethylene glycol: hydrodynamic radius and shape anisotropy. *Biophys. J.* 95(4):1590–99
35. Weill G, Maret G. 1982. Magnetic birefringence of polystyrene sulphonate: molecular weight and concentration dependence. *Polymer* 23(13):1990–93
36. McCulloch B, Ho V, Hoarfrost M, Stanley C, Do C, et al. 2013. Polymer chain shape of poly(3-alkylthiophenes) in solution using small-angle neutron scattering. *Macromolecules* 46(5):1899–907
37. Alexiadis O, Mavrantzas VG. 2013. All-atom molecular dynamics simulation of temperature effects on the structural, thermodynamic, and packing properties of the pure amorphous and pure crystalline phases of regioregular P3HT. *Macromolecules* 46(6):2450–67
38. Mirsakiyeva A, Hugosson HW, Crispin X, Delin A. 2017. Quantum molecular dynamical calculations of PEDOT 12-oligomer and its selenium and tellurium derivatives. *J. Electron. Mater.* 46(5):3071–75
39. Franco-Gonzalez JF, Zozoulenko IV. 2017. Molecular dynamics study of morphology of doped PEDOT: from solution to dry phase. *J. Phys. Chem. B* 121(16):4299–307
40. Patel SN, Javier AE, Stone GM, Mullin SA, Balsara NP. 2012. Simultaneous conduction of electronic charge and lithium ions in block copolymers. *ACS Nano* 6(2):1589–600
41. Merkle R, Gutbrod P, Reinold P, Katzmaier M, Tkachov R, et al. 2017. Mixed conductivity of polythiophene-based ionic polymers under controlled conditions. *Polymer* 132:216–26
42. Shiri P, Dacanay EJS, Hagen B, Kaake LG. 2019. Vogel-Tammann-Fulcher model for charging dynamics in an organic electrochemical transistor. *J. Mater. Chem. C* 7(41):12935–41
43. Finn PA, Jacobs IE, Armitage J, Wu R, Paulsen BD, et al. 2020. Effect of polar side chains on neutral and p-doped polythiophene. *J. Mater. Chem. C* 8:16216–23
44. Dong BX, Nowak C, Onorato JW, Strzalka J, Escobedo FA, et al. 2019. Influence of side-chain chemistry on structure and ionic conduction characteristics of polythiophene derivatives: a computational and experimental study. *Chem. Mater.* 31(4):1418–29
45. Chee KJ, Kumar V, Nguyen CV, Wang J, Lee PS. 2016. Polymer light-emitting electrochemical cell blends based on selection of lithium salts, LiX [X = trifluoromethanesulfonate, hexafluorophosphate, and bis(trifluoromethylsulfonyl)imide] with low turn-on voltage. *J. Phys. Chem. C* 120(21):11324–30
46. Javier AE, Patel SN, Hallinan DT, Srinivasan V, Balsara NP. 2011. Simultaneous electronic and ionic conduction in a block copolymer: application in lithium battery electrodes. *Angew. Chem. Int. Ed.* 50(42):9848–51
47. Bhatt MP, Thelen JL, Balsara NP. 2015. Effect of copolymer composition on electronic conductivity of electrochemically oxidized poly(3-hexylthiophene)-*b*-poly(ethylene oxide) block copolymers. *Chem. Mater.* 27(14):5141–48
48. Miller TF, Wang Z-G, Coates GW, Balsara NP. 2017. Designing polymer electrolytes for safe and high capacity rechargeable lithium batteries. *Acc. Chem. Res.* 50(3):590–93
49. Lévesque I, Bazinet P, Roovers J. 2000. Optical properties and dual electrical and ionic conductivity in poly(3-methylhexa(oxyethylene)oxy-4-methylthiophene). *Macromolecules* 33(8):2952–57
50. Lin F, Wang Y, Lonergan M. 2008. Ion transport in polyacetylene ionomers. *J Appl. Phys.* 104(10):103517
51. Collins SD, Mikhnenko OV, Nguyen TL, Rengert ZD, Bazan GC, et al. 2017. Observing ion motion in conjugated polyelectrolytes with Kelvin probe force microscopy. *Adv. Electron. Mater.* 3(3):1700005

52. Wieland M, Dingler C, Merkle R, Maier J, Ludwigs S. 2020. Humidity-controlled water uptake and conductivities in ion and electron mixed conducting polythiophene films. *ACS Appl. Mater. Interfaces* 12(5):6742–51
53. Xue Z, He D, Xie X. 2015. Poly(ethylene oxide)-based electrolytes for lithium-ion batteries. *J. Mater. Chem. A* 3(38):19218–53
54. Yang C, Sun Q, Qiao J, Li Y. 2003. Ionic liquid doped polymer light-emitting electrochemical cells. *J. Phys. Chem. B* 107(47):12981–88
55. Armel V, Rivnay J, Malliaras G, Winther-Jensen B. 2013. Unexpected interaction between PEDOT and phosphonium ionic liquids. *J. Am. Chem. Soc.* 135(30):11309–13
56. Nardes AM, Kemerink M, de Kok MM, Vinken E, Maturova K, Janssen RAJ. 2008. Conductivity, work function, and environmental stability of PEDOT:PSS thin films treated with sorbitol. *Org. Electron.* 9(5):727–34
57. Spyropoulos GD, Gelinas JN, Khodagholy D. 2019. Internal ion-gated organic electrochemical transistor: a building block for integrated bioelectronics. *Sci. Adv.* 5(2):eaau7378
58. Cao Y, Pei Q, Andersson MR, Yu G, Heeger AJ. 1997. Light-emitting electrochemical cells with crown ether as solid electrolyte. *J. Electrochem. Soc.* 144(12):L317
59. Chang WB, Fang H, Liu J, Evans CM, Russ B, et al. 2016. Electrochemical effects in thermoelectric polymers. *ACS Macro Lett.* 5(4):455–59
60. Wang H, Ail U, Gabrielsson R, Berggren M, Crispin X. 2015. Ionic Seebeck effect in conducting polymers. *Adv. Energy Mater.* 5(11):1500044
61. Malti A, Edberg J, Granberg H, Khan ZU, Andreasen JW, et al. 2016. An organic mixed ion-electron conductor for power electronics. *Adv. Sci.* 3(2):1500305
62. Amdursky N, Głowacki ED, Meredith P. 2019. Macroscale biomolecular electronics and ionics. *Adv. Mater.* 31(3):1802221
63. Savva A, Cendra C, Giugni A, Torre B, Surgailis J, et al. 2019. Influence of water on the performance of organic electrochemical transistors. *Chem. Mater.* 31(3):927–37
64. Gladisch J, Stavrinidou E, Ghosh S, Giovannitti A, Moser M, et al. 2020. Reversible electronic solid-gel switching of a conjugated polymer. *Adv. Sci.* 7(2):1901144
65. Flagg LQ, Giridharagopal R, Guo J, Ginger DS. 2018. Anion-dependent doping and charge transport in organic electrochemical transistors. *Chem. Mater.* 30(15):5380–89
66. Surgailis J, Savva A, Druet V, Paulsen BD, Wu R, et al. 2021. Mixed conduction in an n-type organic semiconductor in the absence of hydrophilic side-chains. *Adv. Funct. Mater.* In press. **https://doi.org/10.1002/adfm.202010165**
67. Berry GC. 1978. Properties of an optically anisotropic heterocyclic ladder polymer (BBL) in dilute solution. *J. Polym. Sci. Polym. Symp.* 65(1):143–72
68. Li G, Pickup PG. 2000. Ion transport in poly(3,4-ethylenedioxythiophene)-poly(styrene-4-sulfonate) composites. *Phys. Chem. Chem. Phys.* 2(6):1255–60
69. Stavrinidou E, Leleux P, Rajaona H, Khodagholy D, Rivnay J, et al. 2013. Direct measurement of ion mobility in a conducting polymer. *Adv. Mater.* 25(32):4488–93
70. McFarlane SL, Day BA, McEleney K, Freund MS, Lewis NS. 2011. Designing electronic/ionic conducting membranes for artificial photosynthesis. *Energy Environ. Sci.* 4(5):1700–3
71. Liu J, Davis NR, Liu DS, Hammond PT. 2012. Highly transparent mixed electron and proton conducting polymer membranes. *J. Mater. Chem.* 22(31):15534–39
72. Ispas A, Peipmann R, Bund A, Efimov I. 2009. On the p-doping of PEDOT layers in various ionic liquids studied by EQCM and acoustic impedance. *Electrochim. Acta* 54(20):4668–75
73. Wang S, Li F, Easley AD, Lutkenhaus JL. 2019. Real-time insight into the doping mechanism of redox-active organic radical polymers. *Nat. Mater.* 18(1):69–75
74. Flagg LQ, Bischak CG, Quezada RJ, Onorato JW, Luscombe CK, Ginger DS. 2020. P-type electrochemical doping can occur by cation expulsion in a high-performing polymer for organic electrochemical transistors. *ACS Mater. Lett.* 2(3):254–60
75. Ghosh S, Inganäs O. 1999. Conducting polymer hydrogels as 3D electrodes: applications for supercapacitors. *Adv. Mater.* 11(14):1214–18

76. Dai T, Qing X, Lu Y, Xia Y. 2009. Conducting hydrogels with enhanced mechanical strength. *Polymer* 50(22):5236–41
77. Yao B, Wang H, Zhou Q, Wu M, Zhang M, et al. 2017. Ultrahigh-conductivity polymer hydrogels with arbitrary structures. *Adv. Mater.* 29(28):1700974
78. Lu B, Yuk H, Lin S, Jian N, Qu K, et al. 2019. Pure PEDOT:PSS hydrogels. *Nat. Commun.* 10(1):1043
79. Wilcox DA, Agarkar V, Mukherjee S, Boudouris BW. 2018. Stable radical materials for energy applications. *Annu. Rev. Chem. Biomol. Eng.* 9:83–103
80. Sato K, Ichinoi R, Mizukami R, Serikawa T, Sasaki Y, et al. 2018. Diffusion-cooperative model for charge transport by redox-active nonconjugated polymers. *J. Am. Chem. Soc.* 140(3):1049–56
81. Yu I, Jeon D, Boudouris B, Joo Y. 2020. Mixed ionic and electronic conduction in radical polymers. *Macromolecules* 53(11):4435–41
82. Xu K, Sun H, Ruoko T-P, Wang G, Kroon R, et al. 2020. Ground-state electron transfer in all-polymer donor-acceptor heterojunctions. *Nat. Mater.* 19(7):738–44
83. Sun H, Gerasimov J, Berggren M, Fabiano S. 2018. n-Type organic electrochemical transistors: materials and challenges. *J. Mater. Chem. C* 6(44):11778–84
84. Giovannitti A, Rashid RB, Thiburce Q, Paulsen BD, Cendra C, et al. 2020. Energetic control of redox-active polymers toward safe organic bioelectronic materials. *Adv. Mater.* 32(16):1908047
85. Zozoulenko I, Singh A, Singh SK, Gueskine V, Crispin X, Berggren M. 2019. Polarons, bipolarons, and absorption spectroscopy of PEDOT. *ACS Appl. Polym. Mater.* 1(1):83–94
86. Kroon R, Kiefer D, Stegerer D, Yu L, Sommer M, Müller C. 2017. Polar side chains enhance processability, electrical conductivity, and thermal stability of a molecularly p-doped polythiophene. *Adv. Mater.* 29(24):1700930
87. Kiefer D, Kroon R, Hofmann AI, Sun H, Liu X, et al. 2019. Double doping of conjugated polymers with monomer molecular dopants. *Nat. Mater.* 18(2):149–55
88. Shi H, Liu C, Jiang Q, Xu J. 2015. Effective approaches to improve the electrical conductivity of PEDOT:PSS: a review. *Adv. Electron. Mater.* 1(4):1500017
89. Kang K, Watanabe S, Broch K, Sepe A, Brown A, et al. 2016. 2D coherent charge transport in highly ordered conducting polymers doped by solid state diffusion. *Nat. Mater.* 15(8):896–902
90. Fratini S, Nikolka M, Salleo A, Schweicher G, Sirringhaus H. 2020. Charge transport in high-mobility conjugated polymers and molecular semiconductors. *Nat. Mater.* 19(5):491–502
91. Xia Y, Cho JH, Lee J, Ruden PP, Frisbie CD. 2009. Comparison of the mobility-carrier density relation in polymer and single-crystal organic transistors employing vacuum and liquid gate dielectrics. *Adv. Mater.* 21(21):2174–79
92. Paulsen BD, Frisbie CD. 2012. Dependence of conductivity on charge density and electrochemical potential in polymer semiconductors gated with ionic liquids. *J. Phys. Chem. C* 116(4):3132–41
93. Stevens DM, Qin Y, Hillmyer MA, Frisbie CD. 2009. Enhancement of the morphology and open circuit voltage in bilayer polymer/fullerene solar cells. *J. Phys. Chem. C* 113(26):11408–15
94. Jiang X, Harima Y, Yamashita K, Tada Y, Ohshita J, Kunai A. 2002. Doping-induced change of carrier mobilities in poly(3-hexylthiophene) films with different stacking structures. *Chem. Phys. Lett.* 364(5):616–20
95. Kuroda S, Marumoto K, Sakanaka T, Takeuchi N, Shimoi Y, et al. 2007. Electron-nuclear double-resonance observation of spatial extent of polarons in polythiophene and poly(3-alkylthiophene). *Chem. Phys. Lett.* 435(4):273–77
96. Trefz D, Ruff A, Tkachov R, Wieland M, Goll M, et al. 2015. Electrochemical investigations of the n-type semiconducting polymer P(NDI_2OD-T_2) and its monomer: new insights in the reduction behavior. *J. Phys. Chem. C* 119(40):22760–71
97. Wang S, Sun H, Ail U, Vagin M, POÅ Persson, et al. 2016. Thermoelectric properties of solution-processed n-doped ladder-type conducting polymers. *Adv. Mater.* 28(48):10764–71
98. Ghosh R, Pochas CM, Spano FC. 2016. Polaron delocalization in conjugated polymer films. *J. Phys. Chem. C* 120(21):11394–406
99. Thomas TH, Harkin DJ, Gillett AJ, Lemaur V, Nikolka M, et al. 2019. Short contacts between chains enhancing luminescence quantum yields and carrier mobilities in conjugated copolymers. *Nat. Commun.* 10(1):2614

100. Bucella SG, Luzio A, Gann E, Thomsen L, McNeill CR, et al. 2015. Macroscopic and high-throughput printing of aligned nanostructured polymer semiconductors for MHz large-area electronics. *Nat. Commun.* 6(1):8394
101. Himmelberger S, Vandewal K, Fei Z, Heeney M, Salleo A. 2014. Role of molecular weight distribution on charge transport in semiconducting polymers. *Macromolecules* 47(20):7151–57
102. Gu K, Snyder CR, Onorato J, Luscombe CK, Bosse AW, Loo Y-L. 2018. Assessing the Huang-Brown description of tie chains for charge transport in conjugated polymers. *ACS Macro Lett.* 7(11):1333–38
103. Dong BX, Liu Z, Misra M, Strzalka J, Niklas J, et al. 2019. Structure control of a π-conjugated oligothiophene-based liquid crystal for enhanced mixed ion/electron transport characteristics. *ACS Nano* 13(7):7665–75
104. Parr ZS, Rashid RB, Paulsen BD, Poggi B, Tan E, et al. 2020. Semiconducting small molecules as active materials for p-type accumulation mode organic electrochemical transistors. *Adv. Electron. Mater.* 6(6):2000215
105. Harima Y, Eguchi T, Yamashita K. 1998. Enhancement of carrier mobilities in poly(3-methylthiophene) by an electrochemical doping. *Synth. Met.* 95(1):69–74
106. Hulea IN, Brom HB, Houtepen AJ, Vanmaekelbergh D, Kelly JJ, Meulenkamp EA. 2004. Wide energy-window view on the density of states and hole mobility in poly(*ρ*-phenylene vinylene). *Phys. Rev. Lett.* 93(16):166601
107. Rivnay J, Inal S, Collins BA, Sessolo M, Stavrinidou E, et al. 2016. Structural control of mixed ionic and electronic transport in conducting polymers. *Nat. Commun.* 7:11287
108. Kim S-M, Kim C-H, Kim Y, Kim N, Lee W-J, et al. 2018. Influence of PEDOT:PSS crystallinity and composition on electrochemical transistor performance and long-term stability. *Nat. Commun.* 9(1):3858
109. Tordera D, Kuik M, Rengert ZD, Bandiello E, Bolink HJ, et al. 2014. Operational mechanism of conjugated polyelectrolytes. *J. Am. Chem. Soc.* 136(24):8500–3
110. Patel SN, Javier AE, Balsara NP. 2013. Electrochemically oxidized electronic and ionic conducting nanostructured block copolymers for lithium battery electrodes. *ACS Nano* 7(7):6056–68
111. Kim N, Kee S, Lee SH, Lee BH, Kahng YH, et al. 2014. Highly conductive PEDOT:PSS nanofibrils induced by solution-processed crystallization. *Adv. Mater.* 26(14):2268–72
112. Nikolka M, Broch K, Armitage J, Hanifi D, Nowack PJ, et al. 2019. High-mobility, trap-free charge transport in conjugated polymer diodes. *Nat. Commun.* 10(1):2122
113. Kergoat L, Piro B, Berggren M, Horowitz G, Pham M-C. 2012. Advances in organic transistor-based biosensors: from organic electrochemical transistors to electrolyte-gated organic field-effect transistors. *Anal. Bioanal. Chem.* 402(5):1813–26
114. Kim SH, Hong K, Xie W, Lee KH, Zhang S, et al. 2013. Electrolyte-gated transistors for organic and printed electronics. *Adv. Mater.* 25(13):1822–46
115. Zeglio E, Inganäs O. 2018. Active materials for organic electrochemical transistors. *Adv. Mater.* 30(44):1800941
116. Moser M, Ponder JF, Wadsworth A, Giovannitti A, McCulloch I. 2019. Materials in organic electrochemical transistors for bioelectronic applications: past, present, and future. *Adv. Funct. Mater.* 29(21):1807033
117. Inal S, Malliaras GG, Rivnay J. 2017. Benchmarking organic mixed conductors for transistors. *Nat. Commun.* 8(1):1767
118. Friedlein JT, McLeod RR, Rivnay J. 2018. Device physics of organic electrochemical transistors. *Org. Electron.* 63:398–414
119. Lin P, Yan F, Chan HLW. 2010. Ion-sensitive properties of organic electrochemical transistors. *ACS Appl. Mater. Interfaces* 2(6):1637–41
120. Romele P, Ghittorelli M, Kovács-Vajna ZM, Torricelli F. 2019. Ion buffering and interface charge enable high performance electronics with organic electrochemical transistors. *Nat. Commun.* 10(1):3044
121. Mochizuki Y, Horii T, Okuzaki H. 2012. Effect of pH on structure and conductivity of PEDOT/PSS. *Trans. Mater. Res. Soc. Jpn.* 37(2):307–10
122. Savva A, Wustoni S, Inal S. 2018. Ionic-to-electronic coupling efficiency in PEDOT:PSS films operated in aqueous electrolytes. *J. Mater. Chem. C* 6(44):12023–30

123. Paulsen BD, Wu R, Takacs CJ, Steinrück H-G, Strzalka J, et al. 2020. Time-resolved structural kinetics of an organic mixed ionic-electronic conductor. *Adv. Mater.* 32(40):2003404
124. Giovannitti A, Maria IP, Hanifi D, Donahue MJ, Bryant D, et al. 2018. The role of the side chain on the performance of n-type conjugated polymers in aqueous electrolytes. *Chem. Mater.* 30(9):2945–53
125. Savva A, Hallani R, Cendra C, Surgailis J, Hidalgo TC, et al. 2020. Balancing ionic and electronic conduction for high-performance organic electrochemical transistors. *Adv. Funct. Mater.* 30(11):1907657
126. Moser M, Hidalgo TC, Surgailis J, Gladisch J, Ghosh S, et al. 2020. Side chain redistribution as a strategy to boost organic electrochemical transistor performance and stability. *Adv. Mater.* 32(37):2002748
127. Yuk H, Lu B, Zhao X. 2019. Hydrogel bioelectronics. *Chem. Soc. Rev.* 48(6):1642–67
128. Zhang W, Feng P, Chen J, Sun Z, Zhao B. 2019. Electrically conductive hydrogels for flexible energy storage systems. *Prog. Polym. Sci.* 88:220–40
129. Guo Y, Bae J, Fang Z, Li P, Zhao F, Yu G. 2020. Hydrogels and hydrogel-derived materials for energy and water sustainability. *Chem. Rev.* 120(15):7642–707
130. Naficy S, Razal JM, Spinks GM, Wallace GG, Whitten PG. 2012. Electrically conductive, tough hydrogels with pH sensitivity. *Chem. Mater.* 24(17):3425–33
131. Newbloom GM, Weigandt KM, Pozzo DC. 2012. Electrical, mechanical, and structural characterization of self-assembly in poly(3-hexylthiophene) organogel networks. *Macromolecules* 45(8):3452–62
132. Danielsen SPO, Sanoja GE, McCuskey SR, Hammouda B, Bazan GC, et al. 2018. Mixed conductive soft solids by electrostatically driven network formation of a conjugated polyelectrolyte. *Chem. Mater.* 30(4):1417–26
133. Garcia A, Bakus RC II, Zalar P, Hoven CV, Brzezinski JZ, Nguyen T-Q. 2011. Controlling ion motion in polymer light-emitting diodes containing conjugated polyelectrolyte electron injection layers. *J. Am. Chem. Soc.* 133(8):2492–98
134. Ji X, Paulsen B, Chik G, Wu R, Yin Y, et al. 2021. Mimicking associative learning using an ion-trapping non-volatile synaptic organic electrochemical transistor. *Nat. Commun.* 12:2480
135. Jiang Q, Sun H, Zhao D, Zhang F, Hu D, et al. 2020. High thermoelectric performance in n-type perylene bisimide induced by the Soret effect. *Adv. Mater.* 32(45):2002752
136. Bubnova O, Khan ZU, Malti A, Braun S, Fahlman M, et al. 2011. Optimization of the thermoelectric figure of merit in the conducting polymer poly(3,4-ethylenedioxythiophene). *Nat Mater*. 10(6):429–33
137. Patel SN, Glaudell AM, Peterson KA, Thomas EM, O'Hara KA, et al. 2017. Morphology controls the thermoelectric power factor of a doped semiconducting polymer. *Sci. Adv.* 3(6):e1700434
138. Ail U, Jafari MJ, Wang H, Ederth T, Berggren M, Crispin X. 2016. Thermoelectric properties of polymeric mixed conductors. *Adv. Funct. Mater.* 26(34):6288–96
139. Zhao D, Fabiano S, Berggren M, Crispin X. 2017. Ionic thermoelectric gating organic transistors. *Nat. Commun.* 8:14214
140. Li T, Zhang X, Lacey SD, Mi R, Zhao X, et al. 2019. Cellulose ionic conductors with high differential thermal voltage for low-grade heat harvesting. *Nat. Mater.* 18(6):608–13
141. Han C-G, Qian X, Li Q, Deng B, Zhu Y, et al. 2020. Giant thermopower of ionic gelatin near room temperature. *Science* 368(6495):1091–98
142. Kim B, Na J, Lim H, Kim Y, Kim J, Kim E. 2019. Robust high thermoelectric harvesting under a self-humidifying bilayer of metal organic framework and hydrogel layer. *Adv. Funct. Mater.* 29(7):1807549
143. Zhao D, Martinelli A, Willfahrt A, Fischer T, Bernin D, et al. 2019. Polymer gels with tunable ionic Seebeck coefficient for ultra-sensitive printed thermopiles. *Nat. Commun.* 10(1):1093
144. Kim B, Hwang JU, Kim E. 2020. Chloride transport in conductive polymer films for an n-type thermoelectric platform. *Energy Environ. Sci.* 13(3):859–67
145. Glaudell AM, Cochran JE, Patel SN, Chabinyc ML. 2015. Impact of the doping method on conductivity and thermopower in semiconducting polythiophenes. *Adv. Energy Mater.* 5(4):1401072
146. Kang SD, Snyder GJ. 2017. Charge-transport model for conducting polymers. *Nat. Mater.* 16(2):252–57
147. Abdalla H, Zuo G, Kemerink M. 2017. Range and energetics of charge hopping in organic semiconductors. *Phys. Rev. B* 96(24):241202
148. Scheunemann D, Vijayakumar V, Zeng H, Durand P, Leclerc N, et al. 2020. Rubbing and drawing: generic ways to improve the thermoelectric power factor of organic semiconductors? *Adv. Electron. Mater.* 6(8):2000218

149. Wang H, Zhao D, Khan ZU, Puzinas S, Jonsson MP, et al. 2017. Ionic thermoelectric figure of merit for charging of supercapacitors. *Adv. Electron. Mater.* 3(4):1700013
150. Håkansson A, Shahi M, Brill JW, Fabiano S, Crispin X. 2019. Conducting-polymer bolometers for low-cost IR-detection systems. *Adv. Electron. Mater.* 5(6):1800975
151. Weathers A, Khan ZU, Brooke R, Evans D, Pettes MT, et al. 2015. Significant electronic thermal transport in the conducting polymer poly(3,4-ethylenedioxythiophene). *Adv. Mater.* 27(12):2101–6
152. Liu J, Wang X, Li D, Coates NE, Segalman RA, Cahill DG. 2015. Thermal conductivity and elastic constants of PEDOT:PSS with high electrical conductivity. *Macromolecules* 48(3):585–91
153. Wei Q, Mukaida M, Kirihara K, Ishida T. 2014. Experimental studies on the anisotropic thermoelectric properties of conducting polymer films. *ACS Macro Lett.* 3(9):948–52
154. Kim G-H, Kim J, Pipe KP. 2016. Humidity-dependent thermoelectric properties of poly (3,4-ethylenedioxythiophene):poly(styrene sulfonate). *Appl. Phys. Lett.* 108(9):093301

Annual Review of Materials Research

Volume 51, 2021

Contents

Mixed Transport Polymers

Structural Materials

Current Interest

Indexes

Errata

An online log of corrections to *Annual Review of Materials Research* articles may be found at http://www.annualreviews.org/errata/matsci